A Review of Gas-Fed Pulsed Plasma Thruster Research over the Last Half-Century

John K. Ziemer
Electric Propulsion and Plasma Dynamics Lab (EPPDyL)
Princeton University

Introduction

This is summary of gas-fed pulsed plasma thruster (GFPPT) work from the late 1950's until the present year. The scope includes coaxial, parallel-plate, z-pinch and hybrid geometries using ambient fill or pulsed gas injection techniques with hydrogen, nitrogen, argon, and xenon propellants. The topic is generally limited to "pulsed" devices where the total operation time is less than any plasma or current stabilization time, that is, excluding any "quasi-steady" thrusters. Both capacitor and transmission line (lumped inductor-capacitor) energy sources are considered, however, purely inductive discharges are not due to the absence of electrode effects that may be very important in more prevalent GFPPT designs.

This review is divided into three parts according to the place where the research was conducted, the overall subject matter, and then an overview and discussion. In the first part, each section individually covers the work at General Dynamics, General Electric, Lockheed, Republic Aviation, NASA, and Princeton. In the second part, using a combination of repeated information from the previous part as well as new citations from other laboratories, the subjects of current sheet structure and stability (including canting), current sheet acceleration models, theoretical performance scaling, and experimental performance measurement. Both of these parts are designed to stand alone for the convenience of the reader although the first part is designed to provide a much more detailed coverage while the second part is more of a summary. Finally, in the last part, a brief overview of research from over the last half-century and a discussion on the current and future GFPPT research will be presented.

In general, this review tries to make use of peer-reviewed journal publications instead of non-reviewed conference papers or technical reports. Although sometimes these will be used to supplement the information contained in the journal articles, frequently the content is very similar. For each section, there will be a summary of the research data and proposed theories presented in the reviewed articles as well as a separate discussion sub-section consisting of this author's relevant theories and opinions on the topic. Previous reviews of GFPPTs have followed a similar, although perhaps more compressed, format [1, 2, 3]. In this

case, the author is trying to summarize more than simply the best or final results from each group, rather, the history, lineage, progress, and lessons learned along the way are also explained in detail. With this approach, both the reader who is interested in a detailed chronology or a simple summary should both be satisfied.

At this point, it should be noted that with the many ways to measure GF-PPT performance used in the literature including calorimetry, ballistic pendulums, streak and Kerr-cell photographs, electric probes, and thrust stands, only the thrust stand provides a direct measurement that has been accepted by the research community [2] and is not influenced by assumptions of sweeping efficiency, initial propellant density distribution, ionization fraction, etc. However, this technique along with all the others are susceptible to the influences of adsorbed gas and organic mono-layers on the electrode surfaces [4, 5] common to many vacuum facilities and pump-down procedures. Except where noted, the author will *only* use thrust stand data to *compare* performance (impulse, specific impulse, thrust-to-power ratio, efficiency) while elucidating the degree to which, if at all, the investigators took into account the possibility of this type of contamination in their observations.

Part I
Research by Laboratory

1 General Dynamics

D.E.T.F. Ashby, R. Dethlefsen, T.J. Gooding, B.R. Hayworth, A.V. Larson, L. Liebing, R.H. Lovberg, and L.C. Burkhardt (Los Alamos). ***1962-1966***

Burkhardt and Lovberg began researching "plasma guns" (see Ref. [6]) as a high velocity source of plasma for fusion research in 1962 at Los Alamos [7]. Investigating a coaxial geometry, they used deuterium for propellant that was controlled and radially injected by a solenoid valve through ports approximately half-way down the center electrode. Fast ion-gauge pressure measurements showed that the propellant distribution was relatively gaussian around the injection ports (with all the propellant contained within the electrode volume) just before the discharge. The discharge was initiated when the pressure between the electrodes became high enough for a Paschen breakdown. The overall density and mass bit were controlled by the plenum pressure upstream of the solenoid valve. Depending on pressure, the breakdown occurred near the breach (low pressure with long times before paschen breakdown) or near the propellant ports (high pressure with almost immediate breakdown, frequently asymmetric) [8]. For this accelerator design, the center electrode was the cathode ($r_{outer} = 4.7$ cm, $r_{inner} = 2.5$ cm, radius ratio= 1.88) using a 15 μF capacitor bank charged to 16 kV (1.92 kJ) for each pulse. At a low-pressure test condition

using about 40 μg of propellant, the peak current (110 kA) was reached in 0.7 μs suggesting about 100 nH of parasitic inductance and yielding a very oscillatory current waveform.

At these conditions, the sheet speed was observed to asymptote to 125 km/s indicating that the current sheet was permeable and not acting like a "snow-plow". An effective sweeping efficiency of 50% was estimated based on a predicted computer model of the acceleration process. The peak current and current density were observed to decrease monotonically with decreasing initial propellant density. Electric field probe data showed that the radial electric field was close to zero, which is to say that almost the entire capacitor potential was taken up by the expanding magnetic fields and back emf with almost no resistive voltage drop, only 80 V out of 16 kV. Other E-probe data showed that an *axial* electric field exists within the current sheet, along the direction of acceleration. The average value of the integrated axial field, 167 V, is just enough to predict ion velocities of 125 km/s if only half the ions were accelerated to that speed (consistent with a 50% sweeping efficiency). The axial field value was less near the outer electrode (anode), only 50 V, which is consistent with the $1/r^2$ Lorentz force profile, however, the current sheet itself was seen to be very planar from magnetic field data at different radii. The authors suggested this was either due to higher propellant densities near the center electrode or possibly because of increased ion current near the anode with more research being indicated. Lovberg conducted the same kind of measurements using nitrogen and argon in the same device at a later time and found similar, permeable, shock-like behavior [9].

In 1963 Lovberg joined General Dynamics and continued his work along with Gooding and Hayworth on GFPPTs for propulsion applications. They developed a similar GFPPT design using, again, radial propellant injection (this time, located closer to the backplate) and paschen breakdown initiation [8]. The thruster was slightly smaller with $r_{outer} = 3.8$ cm, $r_{inner} = 1.9$ cm, and radius ratio= 2 with a 5 μF capacitor bank charged between 10-20 kV (0.25-1.0 kJ) for each pulse. At low mass bits they once again reached 10^5 m/s sheet speeds, however spoking instabilities made measurements at higher mass bits difficult to interpret with streak photos. They suggested that when a GFPPT has a "slug-like" propellant distribution, as one would like for dynamic efficiency considerations, it is subject to spoking instabilities. Also, they suspected that their stainless-steel electrodes contributed to the spoking by forming residual "magnetic spots" where the current-spoke would always return. They tested this theory by rotating the center electrode and observing that the spoke attachment followed the rotation[1]

Subsequent thruster designs used more injection ports that were equally spaced down the center electrode to provide a more uniform propellant fill [11] (see Figure 1). General Dynamics also developed their own capacitor with distributed internal inductance to give more of a square-wave current pulse (200 kA

[1]Author's note: this could have also been caused by the propellant distribution coming from the cathode propellant injection ports. If one injection port was favored over another yielding a slightly higher mass flow rate and pressure, the spoking instability might follow that injection port. This has been noticed in other GFPPTs more recently as well [10].

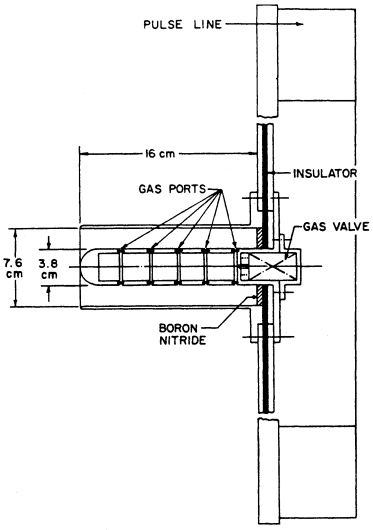

Figure 1: Schematic drawing of General Dynamics GFPPT. Taken from Ref. [11].

peak). With a total capacitance of 22 μF charged to 6.3 kV (437 J) and using nitrogen for propellant, they measured sheet velocities of 10^5 m/s and 30% efficiency from a calorimeter. They also saw a significant improvement in performance by reducing the electrode length from 13 to 8 cm, largely attributed to decreased wall loses. The 30% efficiency point was taken with the shorter electrodes which were "tuned" so that the discharge reaches the end of the electrodes when the current crosses through zero. These measurements of sheet velocity suggested that the current sheet in this thruster *did* behave as a snowplow with close to a 100% sweeping efficiency. Faraday cups placed into the exhaust beams measured ion velocities consistent with the previous sheet speed measurements and calorimetry data [12]. The losses in this thruster were attributed to low dynamic efficiency and the inability to recover much, if any, thermal energy in the plasma as a significant fraction of it was thought lost through inelastic electron-ion collisions and the subsequent radiation [13].

In 1964 Lovberg began experiments investigating the current sheet structure including the use of Schlieren photography [14, 15]. In the first set of experiments [14], a parallel-plate geometry was studied for the ease of optical access. With a height of 3.8 cm and a width of 8 cm, Lovberg believed that field fringing effects would be negligible due to the small aspect ratio of less than two. The accelerator was powered by a 3 μF capacitor charged to 16 kV (384 J) with about 64 nH of measured parasitic inductance. The accelerator exhausted into a small vacuum chamber with the entire volume prefilled to 0.3 Torr of hydrogen (26 μg in 6 cm long electrode volume, $n_0 = 10^{16}$ cm^{-3}). The speed of the

first current sheet was measured using photographs at 80 km/s which agreed well with a snowplow model and 100% sweeping efficiency. The second sheet, coming from the second period of current oscillation, traveled at 110 km/s with barely any density gradient detectable by the Schlieren system suggesting that the first sheet had indeed swept up most of the gas between the electrodes.

The Schlieren photographs showed a very planar, thin (0.5 to 1 cm) current sheet with electron densities of 10^{17} cm^{-3} (about 10 times larger than the initial ambient fill) indicating that most of the propellant mass was compressed into a thin layer as a snowplow model would suggest. There were also strong density gradients observed in a very thin layer all along the cathode suggesting that a small part of the plasma was being left behind there. Lovberg speculated that the electrons are trapped in their gyro-orbits and cannot conduct sufficient current to the cathode. He believed that either the cathode would have to be emitting a large amount of electrons to make up for this lack of conduction or that the ions were conducting a bulk of the current near the cathode producing a larger, localized density. Finally, Lovberg noticed that the sheet began to "bifurcate" as the electrodes became more and more "discolored" from each pulse[2]. Cleaning the electrode corrected the problem, however, in tests with nitrogen, the bifurcation always existed with a thin, diagonal sheet leading the main sheet at the anode. He suggested this was "almost certainly related to the larger ion gyro-radius" of the molecules with no further explanation.

His second Schlieren experiment used a specially designed coaxial electrode set with a slotted outer electrode for optical access [15]. Again, the slightly larger thruster (r_{outer} = 7.5 cm, r_{inner} = 2.5 cm, radius ratio= 3) was backed with the same 3 μF capacitor charged to 16 kV (384 J) to produce a 10^5 A peak current oscillatory waveform. The ambient hydrogen density, however, was very high for this large electrode set giving about 250 μg within the discharge volume. Still, the current sheet reached the end of the electrodes in about 1 μs (6.5 cm long, 65,000 km/s on average) just as the current was crossing through zero.

For the coaxial thruster, the Schlieren photographs showed a very complex distribution of density with a parabolic shaped front centered on the center electrode (anode) followed closely by a ticker, planar front, as shown in Figure 2. Throughout the course of the discharge, the parabolic front moved out ahead of the planar front (120 km/s compared to 50 km/s) while the planar front's thickness increased. Although reversing polarity showed minimal effects (the parabolic front always moved out on the center electrode faster), when the center electrode was negatively charged (cathode) the planar front became much more diffuse. In both cases, the parabolic front moved much faster than expected ($> 2x$) from a snowplow model with the ambient mass density, although it did have the shape expected from the non-uniform Lorentz force. The parabolic front was also found to contain between 80-90% of the current with B-dot probes. Plasma densities were estimated to be about 10^{16} cm^{-3}, almost the same as ambient conditions. Once again, Lovberg reached the conclusion that the current sheet

[2]Please see the following discussion subsection for a possible contamination concern of these measurements

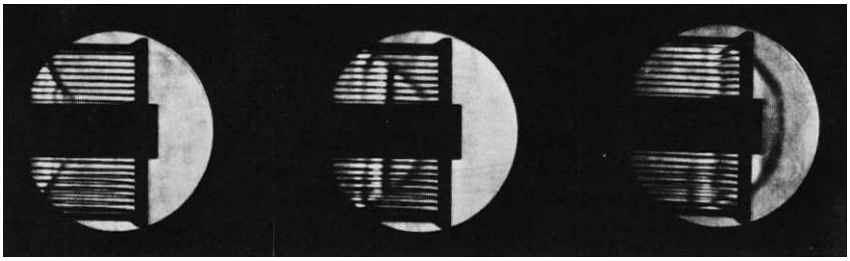

Figure 2: Schlieren photographs taken of discharge in slotted, coaxial accelerator using hydrogen propellant at 0.5, 0.7 and 1.0 μs (left to right) after initiation. These figures show positive polarity (center electrode is anode). Taken from Ref. [15].

in this thruster was permeable and did not act like a perfect snowplow, rather like a strong shock-wave. Lovberg also saw large radial density gradients near the outer electrode (cathode) which could have been caused by either plasma leaking through the optical access slits or by plasma building up near the outer electrode (cathode) walls. Finally, shortening the center electrode had relatively no effect on the plasma front shape or speed with the pinch column beyond the shorter electrode forming a "virtual electrode" with strong radial density gradients.

Lovberg's final current sheet structure experiment used both a capacitor driven discharge with parallel-plate electrodes, and an inductively driven theta-pinch that sought to eliminate the effects of electrodes altogether [16]. As the second apparatus showed very different behavior than conventional discharges with electrodes, those results will not be included here. Returning to the parallel-plate geometry for its more efficient snowplow behavior and one-dimensional nature, Lovberg used electric field and B-dot probes to infer current conduction through a generalized Ohm's law. Assuming the gas is already fully ionized and in the moving reference frame of the current sheet:

$$\vec{E} + \vec{v}_i \times \vec{B} - \frac{1}{n_e e}\left[\vec{j} \times \vec{B} - \nabla p_e\right] - \eta \vec{j} = 0, \tag{1}$$

which includes the Hall effect. Using a right-handed coordinate system with the z-axis in the direction of current sheet motion and the x-axis perpendicular to the electrode surfaces, the vector equation can be broken down into two equations,

$$E_z + v_{ix} B_y - \frac{1}{n_e e}\left[j_x B_y - \frac{\partial p_e}{\partial z}\right] = 0, \tag{2}$$

$$E_x - v_{sheet} B_y - \eta j_x = 0, \tag{3}$$

with the following assumptions: uniformity in the y-direction and current carried only in the x-direction. Neglecting ion current and assuming the pressure

gradient is small,

$$n_e e E_z = j_x B_y. \tag{4}$$

This relation infers that the electron current creates an axial Hall electric field which subsequently accelerates the ions. Lovberg goes on to say that, in general, GFPPTs could be called "pulsed Hall accelerators". If the current sheet itself is the ionization source, then Lovberg postulates a slightly different story. Upon entering the sheet, a neutral atom is ionized and both particles begin to rotate about their gyro-centers in the strong magnetic field. Without collisions and assuming that the thruster geometry dimensions are much bigger than the ion gyro-radius, the separation of the ion and electron gyro-centers in the x-direction will cause a displacement current proportional to the rate at which the sheet picks up and ionizes more atoms. In this case, there is no polarization field (the gyro-centers do not separate in the axial direction), and both the ions and electrons effectively carry the current and feel a Lorentz force on ion cyclotron time scales. Near the electrodes, the finite gyro-radius effects dominate with a high voltage sheath required to bring in electrons near the anode, and an axial electric field developing near the cathode where the ions cannot complete a full gyro-orbit. Qualitatively, Lovberg found this to be the case using hydrogen, with strong density gradients near the cathode and about a 100 V sheath near the anode. Using Nitrogen, or any other higher molecular weight propellant, however, he found that "electrode effects" dominated the discharge pattern as the gyro-radius for the ions became on the same order as the thruster's electrode spacing.

The last two publications from General Dynamics included a summary of the work from 1963-1965 in a NASA contract report [17] and a final journal paper which suggested that a longer, quasi-steady discharge would have a higher efficiency while still benefitting from the arbitrary low power consumption due to the pulsed nature of the device [18]. Without going into further details of the quasi-steady thruster development, and without repeating the information already provided above, the contract report brought out the following points that were not published elsewhere:

- Spoking and other discharge initiation instabilities went away when the dependence on gas pressure and corresponding paschen breakdown to control the initiation timing was removed with the addition of an gas-discharge switch.
- Efficiency of uniformly filled thrusters never exceeded 50% due to dynamic efficiency (calorimetry data).
- A steady-state thrust stand was develop and showed that with pulsed, non-uniform, gas injection the efficiency could be greater than 50%.
- Confirmed Guman's discovery (Ref. [4] of impulse decay with successive pulses and took thrust stand data accordingly, after at least 100 pulses.

- Used a limited number of different charging voltages and gas pressures to determine optimum operating conditions from thrust stand measurements using nitrogen and xenon (see next subsection for a summary of performance data.)
- Found that calorimetry data over-estimated the performance by a significant amount due to inclusion of plasma internal energy captured by calorimeter that is not recovered as thrust.
- The average axial velocity of ions in the exhaust was found to be *greater* than the average velocity calculated from thrust measurements by as much as a factor of two.
- Duplicated General Electric's A-7D thruster (see next section on work at GE) in geometry, capacitance level, propellant delivery, and discharge initiation scheme to find it delivered only about 1/3-1/2 the reported performance.

1.1 Summary of GD Performance Measurements

The measurements presented here were performed during the later stages of GFPPT development at General Dynamics [17] using a thrust stand (pulsed operation at 10 Hz gave effective "steady" measurement and average impulse bit) and an appropriately conditioned thruster to eliminate contamination effects. The capacitance was increased to a final value of 140 μF with a distributed inductance giving nearly a square current pulse. The geometry of this thruster was slightly different than that of Figure 1. The length of the center electrode was shorter (5.5 cm) with the same radius (1.9 cm) while the outer electrode was about the same length (15.8 cm) but had a larger radius (6.25 cm). The new radius ratio was about 3.3. The propellant was injected radially at the breech with the discharge initiation timing controlled by a gas-discharge switch. Propellant utilization was measured to be just over 60% with nitrogen and a 350 μs delay. The mass bit was controlled by changing the feed pressure and the quantity was determined by integrating measured density profiles. Both nitrogen and xenon data were used in this study as shown in Tables 1 and 2 and Figures 3 and 4. In general, the efficiency varied from 6 to 56%, the specific impulse varied from 350 to 13,000 s, and the thrust-to-power ratio varied from 33.5 to 8.7 μN/W, respectively, depending mass bit and energy. As expected, the highest efficiencies corresponded to the highest energy and lowest mass bit values, however, the thrust-to-power ratio is *largest* at the *lowest* energy and highest mass bit values.

Thrust stand data was also obtained using a GFPPT very similar in design to General Electric's A-7D GFPPT with axial propellant flow (xenon) and a separate high-voltage discharge initiation system. GE's mass injection scheme was duplicated very closely to insure the same propellant utilization ($> 90\%$) and density profiles. While faraday cup measurements of ion velocity and exhaust beam divergence were very similar to those obtained at GE (see next section),

thrust stand and performance measurement data disagreed with significantly lower values measured at General Dynamics [17]. Table 3 shows performance values at four energy levels. For this device, the efficiency is relatively constant at a fixed energy while the thrust-to-power ratio still shows a tendency to *decrease* with *increasing* energy and decreasing mass bit.

1.2 Discussion of Research at GD

The research at General Dynamics can be broken into two related subject areas: current sheet studies (mainly conducted by Lovberg) and performance studies.

Current Sheet Studies. In the current sheet studies, Lovberg used electric field and B-dot probes [7, 9] as well as Schlieren photography to investigate the nature of the current sheet and acceleration process in both parallel-plate [14] and coaxial [15] geometries using mainly hydrogen for propellant. One of the main questions he was trying to answer was if the current sheet behaved as a snowplow or a strong shock-wave.

In the parallel-plate geometry, he saw a very planar, thin current sheet that had an electron density ten times that of the ambient pre-pulse density. In addition, probe data on arrival time agreed well with the visual indications of the front. He concluded that the sheet *did* behave as a snowplow effectively sweeping up all the gas in front of it. He also found that there was a strong polarization field and speculated that the electrons were conducting all of the current, experiencing a Lorentz force which then slightly separated them from the ions. The polarization field that develops as a result of this separation was measured to be enough to explain the subsequent ion acceleration. Using gases such as nitrogen and argon he saw the sheet "bifurcate" with the bulk of the current being carried on a canted sheet, anode leading cathode. He did not study this phenomenon in depth but suggested that it was a result of the higher molecular weight, and subsequent larger gyro-radii, of nitrogen and argon molecules. It should be noted at this point, however, that the absence of any canting in Lovberg's parallel-plate Schlieren experiments with hydrogen could have been due to surface effects on the electrodes. Lovberg did, in fact, notice the same "bifurcation" in hydrogen after many pulses. He blamed the appearance of this"unstable" behavior on dirty electrodes and cleaned them to find repeatable behavior. Other authors, however, have noticed that discharge behavior only becomes repeatable *after* many pulses due to adsorbed gases collected while the vacuum vessel is exposed to atmosphere and organic monolayers (pump-oil) deposited during pumping [4, 5]. These "contaminants" are blown off the electrode surfaces after a number of pulses, and "cleaning" them as Lovberg did to re-produce the planar sheet would have to include venting the vacuum vessel and going through another pump-down procedure. The extra gas emitted from the surface of the electrodes during a discharge could radically change the overall behavior of the current sheet, especially near the cathode. Still, Lovberg did see the canting using nitrogen and argon by, more than likely, using the

same procedure as in those studies with hydrogen. To date, the effects of the electrode surface condition on current sheet canting are still unresolved.

In the coaxial geometry using hydrogen, nitrogen, and argon, he saw very different features depending on polarity. In some of his earliest papers, Ref. [7, 9], the center electrode was at cathode potential and the current sheet seemed to be planar from field probe measurements. With the sheet speed measured from probe data being about twice that expected from a snowplow model and the fact that the current sheet itself was not bowed due to the $1/r^2$ Lorentz force profile, he concluded that the sheet *did not* behave like a snowplow. Electric field data showed a similar polarization field to that seen in the parallel-plate geometry, however, it dropped off towards the anode. Although this might be expected with a non-uniform Lorentz profile, the polarization field was no longer strong enough for the ions to be accelerated to sheet speed near the anode. Lovberg postulated that that the current sheet was permeable and acted more like a strong shock-wave. In fact, what Lovberg might have been observing was a significant contribution from ion conduction along with a permeable sheet.

In the case of the reverse polarity and using the Schlieren technique with a slotted outer electrode (Ref. [15]), the current sheet was seen to separate into two layers. The leading sheet was seen to bow out along the center electrode as should be expected by the non-uniform Lorentz force in a coaxial accelerator. In the second, planar layer, he saw a much more diffuse region that did not conduct much current, possibly from a small amount of ion conduction to the cathode. Integrating the gradient information from the Schlieren photos showed that the electron density was about the same as the ambient conditions indicating that this again *did not* behave like a snowplow, rather like a strong shock. A possible explanation for this behavior was the possibility of ion conduction to the cathode which could leave a large number of recombined molecules near the cathode moving only with thermal speed, much slower than the sheet speed. The presence of strong radial density gradients near the cathode seemed to agree with that theory, although Lovberg still did not rule out other possibilities corresponding to the electrons carrying all the current.

It is interesting to note that the current rise times are very similar in the two geometries Lovberg tested, however, the current rise per unit width (in the case of a coaxial geometry the average circumference must be used) is very different. To compare the two, consider *unwrapping* the coaxial geometry to make it like a parallel-plate thruster. The effective width is equal to the average circumference of the electrodes. From this comparison, it is easy to see that the effective width of the coaxial electrodes is much greater than the typical parallel-plate geometry. Distributing the same total current over the two geometries, the current density and inductance-per-unit length are much less in the coaxial thruster. Jahn has pointed out that thrusters with current rise rates per unit width of less than $10^{12} A/(m \cdot s)$ have empirically been shown to have less than 100% sweeping efficiency [1]. In the case of Lovberg's experiments, this criteria also holds true: the parallel-plate accelerator has a width of 8 cm and a current rise rate of 250e9 A/s giving about 3e12 A/ms while the coaxial geometry has an average width of 22.6 cm and a current rise rate of 160e9 A/s giving about

0.7e12 A/ms. In accordance with the rule of thumb, the parallel-plate thruster showed behavior like a snowplow while the coaxial geometry did not. In the other coaxial geometry tested at GD, a higher capacitance and smaller average radius electrodes reached current sire rates up to 1.4e12 A/ms [11]. Although the authors did not expressly try to match or exceed this criteria at the time, probe data confirmed that the current sheet was indeed acting like a snowplow in this later coaxial device.

The coaxial thruster tested by Lovberg showed some interesting features depending on polarity. Although Schlieren photos showed a front that seemed to expand depending on the Lorentz force regardless of polarity, electric probe data for the cathode-center configuration showed a very planar current conduction zone. It could be possible that in the negative polarity the non-uniform Lorentz force profile is balanced by some other effect that normally causes canting with the anode leading the cathode. Other researchers have also seen effects from changing the polarity of a coaxial geometry, however, this discussion will be left to Section 7 where all this information can be summarized together.

Performance Studies. The performance studies are well summarized by the previous section and by Ref. al:GDSummary. First, it is important to notice that the instabilities and asymmetries caused by relying on the propellant density to gradually increase and induce a paschen breakdown were completely removed by the addition of a gas switch. There is no reason to think that either a uniform or slug-like initial propellant distribution is inherently more subject to spoking or other instability from a properly initiated discharge. Second, Results from the calorimeter predicted performance greater than what was measured on the thrust stand. By the author's own admittance, thrust stand data is the only true performance indicator. In addition, GD saw the same effects of impulse decay Guman saw at Republic aviation and measured performance accordingly after at least 100 pulses. This lends credence to their data including the performance measurements of a duplicate GE A-7D thruster that were well below published data provided by GE. This will be discussed in more detail in the next section. Finally, unfortunately researchers at GD performed no real *controlled* experiments to see the effects of capacitance and inductance-per-unit-length on performance.

Impulse Bit (mNs)	Mass Bit (μg)	I_{sp} (s)	Energy (J)	T/P Ratio (μN/W)	Efficiency (%)
1.5	29	5,200	158	9.5	24
3.0	124	2,400	158	19.0	23
3.8	348	1,100	158	24.1	13
2.4	29	8,300	280	8.6	36
3.9	126	3,100	280	13.9	22
5.8	348	1,650	280	20.7	17
3.8	29	13,000	438	8.7	56
5.4	113	4,800	438	12.3	30
7.5	348	2,150	438	17.1	18

Table 1: General Dynamics GFPPT Performance using nitrogen. Taken from Ref. [17], runs 46a-46i.

Impulse Bit (mNs)	Mass Bit (μg)	I_{sp} (s)	Energy (J)	T/P Ratio (μN/W)	Efficiency (%)
2.8	120	2,360	158	17.7	21
3.9	543	710	158	24.7	9
5.3	1490	350	158	33.5	6
4.4	120	3,600	280	15.7	28
5.8	543	1,060	280	20.7	11
7.0	1490	460	280	25.0	6
5.4	120	4,500	438	12.3	28
8.1	543	1,500	438	18.5	13
12.1	1490	810	438	27.2	11

Table 2: General Dynamics GFPPT Performance using xenon. Taken from Ref. [17], runs 45a-45i.

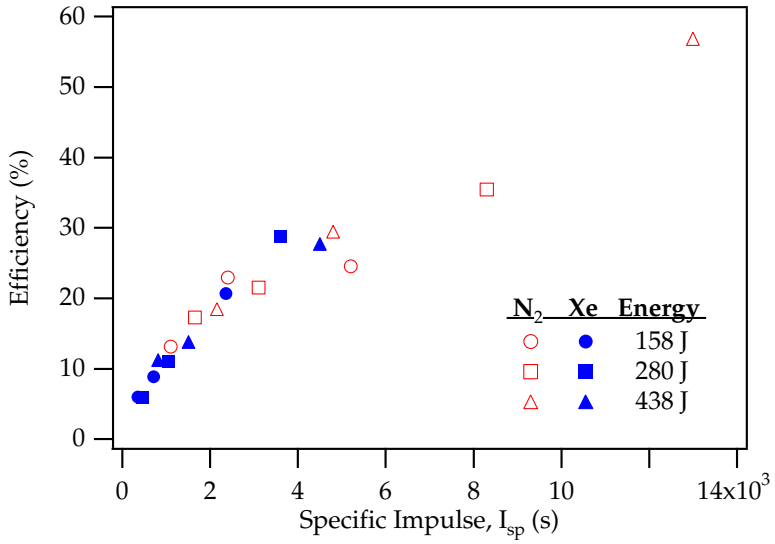

Figure 3: Graph of efficiency vs. specific impulse for the General Dynamics GFPPT. Data taken from Ref. [17] and also presented in Tables 1 and 2.

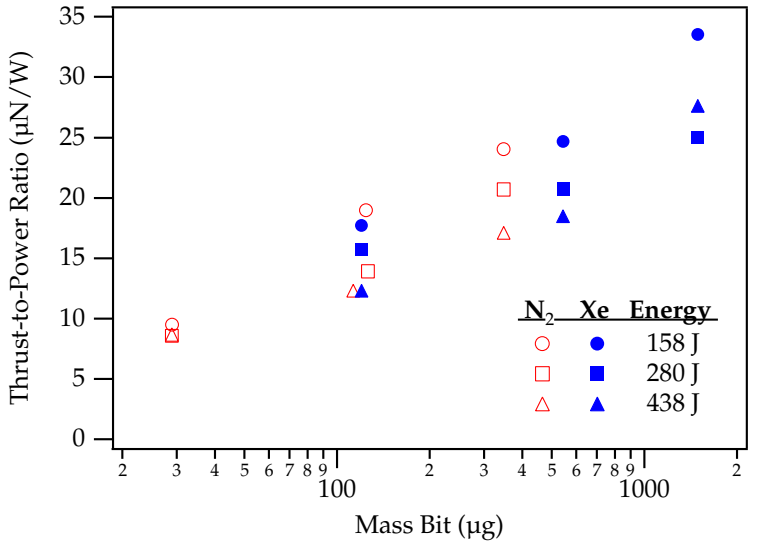

Figure 4: Graph of thrust-to-power ratio vs. mass bit for the General Dynamics GFPPT. Data taken from Ref. [17] and also presented in Tables 1 and 2.

Impulse Bit (mNs)	Mass Bit (μg)	I_{sp} (s)	Energy (J)	T/P Ratio (μN/W)	Efficiency (%)
0.65	29	2,200	63	10.3	11
0.72	35	2,100	63	11.4	12
0.73	52	1,400	63	11.6	8
0.86	29	2,900	109	7.9	12
1.03	35	3,000	109	9.4	14
1.15	29	3,900	158	7.3	14
1.32	35	3,800	158	8.4	16
1.46	52	2,800	158	9.2	13
1.73	69	2,500	158	10.9	14
2.04	98	2,100	158	12.9	13
1.73	29	5,900	280	6.2	18
2.05	42	4,900	280	7.3	18
2.02	47	4,300	280	7.2	16
2.22	52	4,300	280	7.9	17
3.33	98	3,400	280	11.2	20

Table 3: General Dynamics GFPPT Performance using a similar design to GE's A-7D thruster with xenon propellant. Taken from Ref. [17], runs 80-93.

2 General Electric

P. Gloersen, B. Gorowitz, T.W. Karras, J.T. Kenney, and J.H. Rowe.
1963-1970

General Electric started research in 1963 with a long, coaxial accelerator closely resembling the first Marshal (see Ref. [6]) plasma guns [19]. The "Model R" accelerator has a *two-stage* design (similar to a conventional single-stage thruster with a gas switch as the first-stage) and used helium, argon, and most often nitrogen as propellants. The second stage provided most of the acceleration with r_{outer} = 8.75 cm, r_{inner} = 5 cm, radius ratio= 1.75, and length = 47.5 cm from the propellant injection ports (themselves located 7.5 cm from the backplate). Using a 15 μF capacitor bank (for the R-1 and R-2 model) that could be charged up to 13 kV (1.27 kJ) for each pulse, the discharge was initiated with a paschen breakdown in the first stage when the propellant pressure became high enough. Small injection holes allowed some propellant to flow into the main accelerating region before the breakdown in the first stage. With nitrogen flowing at a steady rate of 100 mg/s, according to this author's calculations, only 10% of the propellant remained inside the accelerator at initiation. In this device, peak currents reached 100 kA in about 2 μs with about 90 nH

of parasitic inductance and a very oscillatory current waveform[3]. Calorimetry measurements showed an efficiency of about 12% at 100 J, and increasing the capacitance to 45 μF led to a 26% efficiency at the same voltage. Non-conventional definitions of performance using "energy at terminals" and "effective mass bit", however, made comparing the performance difficult. In addition, although a thrust-stand was operational at this point, it was not used extensively in these first tests.

In 1964, General Electric began parametric performance studies on the effects of changing energy, capacitance, and initial inductance in the Model R accelerators [20]. First, a theoretical model for the acceleration process including a snowplow model for gas accumulation and a circuit equation neglecting the plasma resistance was used to show that reducing the initial inductance would lead to less oscillatory waveforms and better coupling between the driving circuit and the moving discharge. Their model also predicted that efficiency would scale as the inverse of the mass bit with the energy and capacitance kept constant. Increasing energy and capacitance was also found to increase efficiency and specific impulse. Modifications to the Model R gun led to a reduction in initial inductance (15 nH) and improved propellant utilization. Calorimeter measurements showed that the initial inductance drop corresponded to an increase in efficiency up to about 16% at 100 J (an increase by a factor of 1.5). Changes in capacitance (and hence energy at the same voltage) from 15 to 75 μF also improved performance in close to a linear relation. Performance improvements were also seen from increasing the radius ratio, going to a radial instead of axial gas-injection scheme, and shortening the length of the electrodes, especially the inner electrode.

These trends in performance led to the development of the "Model A" guns that were single stage, pulse injected, coaxial accelerators with much shorter electrodes (20-30 cm), large radius ratios (7-10), and even a smaller initial inductance (about 15 nH) that lead to nearly critically damped current waveforms [20]. The "first stage" of the Model R guns was replaced by a small plenum and solenoid valve combination with pulse times of about 100 ms. Please see Table 4 for more details of the accelerator properties and Ref. [20] for a complete account of modifications. Only the most clear and experimentally controlled conclusions will be summarized here.

In the A-1 and A-3 guns, two zones of performance scaling (again measured with calorimetry) were noticed depending on initial capacitor voltage. At lower energies, initial voltages below 4 kV, the efficiency scaled linearly with voltage while at higher energies it remained relatively constant. Again, as the paschen effect controls the breakdown time and hence the amount of propellant that is able to flow before and after the discharge, higher voltages led to *lower* propellant utilization and hence the efficiency stopped increasing even as the discharge energy was increasing. A small collection of calorimeter performance measurements below the voltage cut-off point for the A-1 accelerator with vary-

[3]Author's note: initial inductance measured from the current trace (initial slope) actually gives a *lower* value for the initial inductance close to 45 nH.

Model	r_{inner} (cm)	r_{outer} (cm)	length (cm)	Prop. Injection Area (mm^2)	Capacitance (μF)	Trigger
R-1	5.0	8.75	55	-	15-75	gas
A-1	1.27	8.75	35-20	8.6	15-45	gas
A-3	1.27	12.5	20	8.6	45	gas
A-4(T)	1.27	12.5	20	95	45	gas
A-6	1.27	12.5	20	95	45	elec.
A-7D	1.27	$20^{\dagger}$	20	540	45-145	elec.
A-8D	1.27	$20^{\dagger}$	20	680	45	elec.
A-9D	1.27	$20^{\dagger}$	20	830	45	elec.

Table 4: General Electric accelerator properties, † denotes flared outer electrode from 12.5 to 20 cm over the 20 cm length. Taken from Refs. [20, 21, 22].

ing energy and capacitance are shown in Table 5. The final design mentioned in Ref. [20], the A-4, had a larger radius ratio, and short electrodes, 10 and 20 cm respectively, with the highest reported energy conversion efficiency of 63% using 45 μF charged to 3 kV (203 J). The A-4T modification had a teflon valve seat yielding higher propellant utilization at higher voltages.

Capacitance (μF)	Voltage (kv)	Energy (J)	Efficiency (%)
15	2	30.0	1
45	2	90.0	18
15	3	67.5	13
30	3	135	21
45	3	203	27

Table 5: General Electrics calorimetry measurements for A-1 gun with varying capacitance and initial voltage.

In 1965, based on the success of the A-4 design, GE went through a number of modifications to produce the A-6,A-7D,A-8D, and A-9D models [21]. The major modifications included:

- Electrical triggers (18 kV "pins") were introduced to eliminate initiation timing dependence on paschen breakdown and increase propellant utilization.
- The outer electrode was flared to increase the inductance change and decrease surface effects (surface to volume increased).
- Larger axial injection ports allowed better conductance of gas inside plenum to discharge volume and increased propellant utilization.

In addition, a steady-state thrust stand replaced calorimetric performance measurements with the thruster operating at 10 Hz, and performance measurements taken as average quantities. General Electric's definition of efficiency included a "Q-factor" (depends only on capacitor type) that compensated for internal impedance losses in the capacitor bank. The power supplied to the thruster was defined as,

$$P = \frac{1}{2} C V_0^2 \left(1 - \frac{1}{Q}\right) f_{pulse}. \tag{5}$$

The 45 μF bank described here had a Q-factor of 7 leading to a power that was used in efficiency calculations to be 14% lower than that actually supplied. Erosion measurements showed only 0.25 μg per pulse were lost over 10,000 pulses, and *no* impulse decay or other vacuum facility effect noticed in other labs were reported by GE. The electrode erosion rate was added to the mass flow rate for performance calculations, although this did not significantly alter the results. With the higher propellant utilization efficiencies, *overall* performance increased to $\eta = 70\%$ at 9000 s, 81 J, and 7.4 μg Xe with the A-7D model. Figure 5 shows a schematic drawing of the A-7D model.

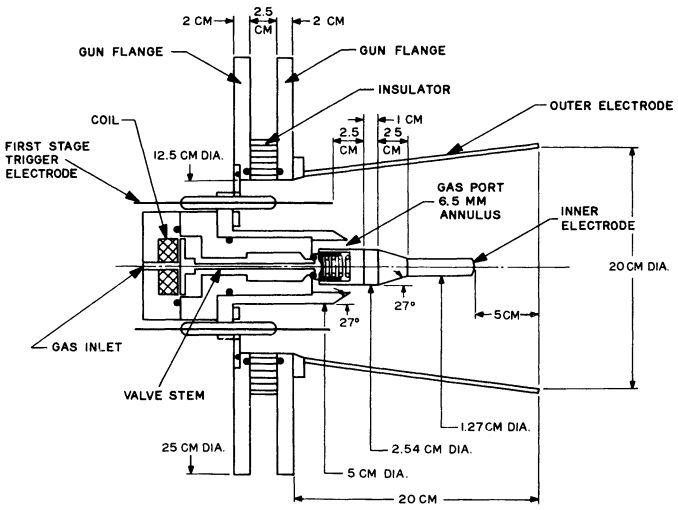

Figure 5: Schematic drawing of General Electrics A-7D GFPPT. Data taken from Ref. [22].

The increase in propellant utilization was explained in more detail in Ref. [22]. Here the evolution of the mass injection system from the A-4T model to the A-9D was presented with the goal of high propellant utilization. The two major changes were to make the injection ports larger for better propellant conductance and to make them face in more of an axial direction to prevent premature self-triggering. Another major contributor to better propellant utilization was

the addition of a fast acting solenoid valve. The the o-ring sealed valve was driven by a 4.4 kV supply permitting a 1 ms cycle time. The discharge was initiated by six 18 kV trigger pins 0.7 ms after the valve cycle was started. With the relatively slow thermal velocity of xenon, over 90% of the gas injected before each pulse remained within the electrode volume for the A-7D model. Fast ion-gauge neutral density measurements were used for the mass utilization efficiency calculation and showed that most of the mass was near the cathode (center electrode) and well away from the backplate. The A-8D and A-9D had similar results, however, not as high of performance with slightly more propellant loaded closer to the cathode for the A-8D and too much propellant ejected too quickly (conductance was too large) in the A-9D.

After 1965, the only reports of GE performance came from conference papers. In Ref. [23], Gorowitz, Gloersen, and Karras defended their A-7D performance measurements with detailed descriptions of experiments (but no tables or graphs of data) that eliminated facility effects (except contamination to this author's satisfaction), thermal drifts in the thrust stand, spurious current conduction to the tank or thrust stand, and contribution from electrode erosion. Once again, a 160 % performance improvement was shown from increasing the capacitance from 45 to 145 μF (the Q-factor of the new capacitor bank was given as 14). During a ten hour test running at 5 Hz (36,000 pulses total), the A-7D model used 30 μg xenon and 65.2 J (950 V) per shot to achieve a 57% overall efficiency with an I_{sp} of 4930 s. The efficiency was seen to scale linearly with specific impulse (constant thrust-to-power ratio of about 20 μN/W) and *not* depend strongly on energy. Similar experiments using nitrogen showed a slightly smaller thrust-to-power ratio of 15 μN/W. A study of changing capacitance showed that efficiency scaled with the square-root of capacitance (within 5-10%) for a constant specific impulse of about 5,000 s. The next subsection gives more measurements with the A-7D model over a variety of mass flow rates and initial voltages. Gorowitz left GE in mid-1966 with his final conference paper providing a mission study using the A-7D which, along with other, later studies, continually quote an efficiency of nearly 60% at 5,000 s [24, 25, 26].

The final journal paper published by GE dealing with GFPPTs was submitted in 1965 and published in 1966 [27]. It described a multi-grid ion collection device that provided measurements of ion velocity and exhaust beam divergence angle with the ability to distinguish between ions of different charge to mass ratios. Although the data agreed with predicted xenon velocities from impulse measurements, carbon and oxygen ions were also present in significant amounts. The amount of these "contaminant" ions varied with each pulse and were not believed to contribute significantly to the thruster impulse.

2.1 Summary of GE Performance Measurements

The measurements provided here in Table 6 and Figures 6 and 7 represent thrust-stand measurements from GE's A-7D model using xenon propellant and a 144.5 μF capacitor bank with a Q-factor of 14. Unfortunately, only energy (with Q-factor reduction), specific impulse, and efficiency were given in Ref. [23]

where all of this data is reported in graphic form. This is, however, the best source for pure data as GE did not frequently show many points in a data set or any tabular presentation. The mass bit and impulse bit values must, therefore, be inferred from the reported specific impulse, voltage, and efficiency measurements,

$$I^*_{bit} = \frac{2\eta}{I_{sp} g_0} \frac{1}{2} C V_0^2 \left(1 - \frac{1}{Q}\right), \tag{6}$$

$$m^*_{bit} = \frac{I^*_{bit}}{I_{sp} g_0}, \tag{7}$$

where the star superscript indicates the inferred quantities. Finally, it must be noted that out of every lab conducting GFPPT performance measurements on thrust stands [4, 5, 17], GE is the *only* one that did not report any decrease in measured thrust or impulse over the first 100-1000 pulses after pump-down, including tests at similar mass bits and energies. As GE's protocol for measuring thrust is not published explicitly except in very early publications, it is unclear if any preconditioning of the thruster took place before the thrust measurements. More on this topic will be discussed in the following subsection.

Impulse Bit (mNs)	Mass Bit (μg)	I_{sp} (s)	Energy (J)	T/P Ratio (μN/W)	Efficiency (%)
0.92	15	6,050	49	18.9	56
0.95	21	4,600	49	19.5	44
1.03	26	4,100	49	21.4	43
1.00	31	3,300	49	20.7	34
1.39	20	7,000	61	23.0	79
1.43	25	5,950	61	23.6	69
1.46	31	4,850	61	24.2	58
1.59	38	4,300	61	26.3	56
1.31	43	3,100	61	21.7	33
1.30	44	3,000	61	21.4	32
2.05	29	7,300	105	19.5	70
2.17	35	6,300	105	20.7	64
2.18	42	5,300	105	20.8	54
2.38	54	4,500	105	22.7	50

Table 6: General Electric A-7D GFPPT Performance with xenon propellant. The impulse bit and mass bit values have been inferred from published efficiency, specific impulse, and energy measurements. Taken from Ref. [23].

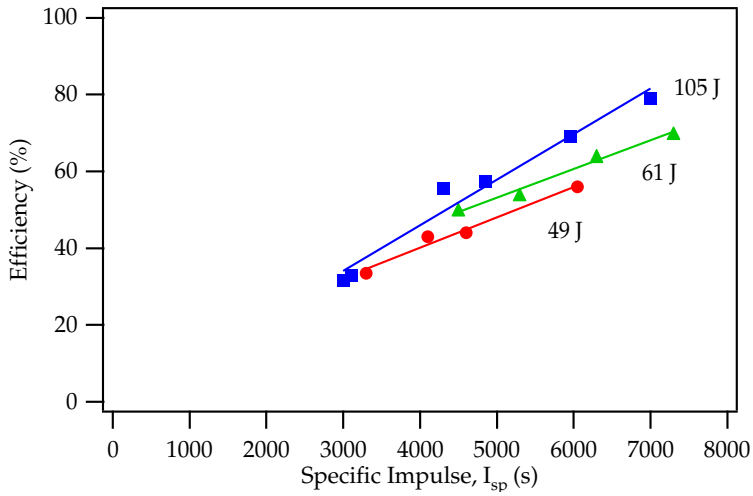

Figure 6: Graph of efficiency vs. specific impulse for the General Electric A-7D GFPPT. Data taken from Ref. [23] and also presented in Table 6.

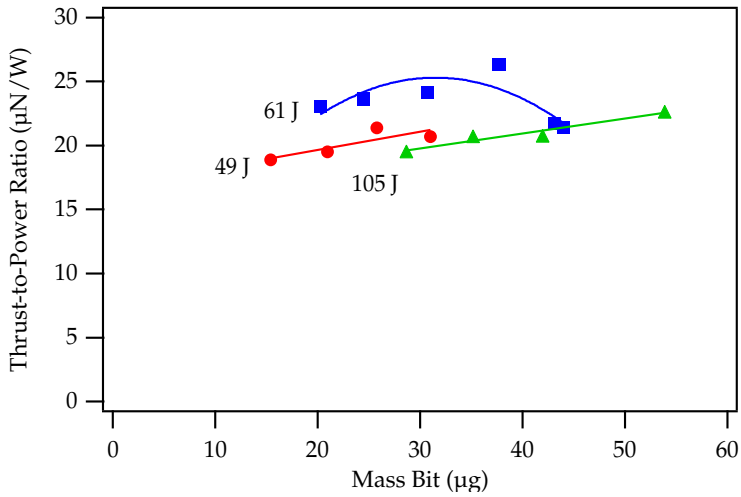

Figure 7: Graph of thrust-to-power ratio vs. mass bit for the General Electric A-7D GFPPT. Data taken from Ref. [23] and also presented in Table 6.

2.2 Discussion of Research at GE

General Electric has reported the highest efficiency measured on a thrust-stand of any GFPPT. After many geometry and propellant injection schemes, their best design, the A-7D, had a large radius ratio of about 16, a 144 μF capacitor bank with only 15 nH of parasitic inductance, and a typical energy per pulse of close to 65 J. Using close to 30 μg of xenon per shot, the efficiency reached 57.5% at a specific impulse of 4850 s. The efficiency was shown to be linear with exhaust velocity over a wide range of mass bits (smaller mass bits gave higher efficiency) with a relatively constant thrust-to-power ratio near 20 μN/W. The propellant utilization efficiency of this design exceeded 90% as a result of using primarily axial injection near the cathode, a 1 ms high-voltage solenoid valve, and separate discharge initiation timing allowed by using six 18 kV trigger pins. GE also conducted a performance survey over five different capacitance values from 50 to 200 μF to find that the performance scaled with the square-root of the capacitance to within 5-10%.

Unfortunately, the researchers at GE did not mention any impulse decay effects that have been observed at three other laboratories testing the performance of GFPPTs on thrust-stands in diffusion pumped chambers [4, 5, 17]. Although researchers at GE did not notice any performance changes from changing the pulse frequency, details of the this experiment and its results were not given. It should be noted that rather than pulse *rate*, the *total number* of pulses has been shown to be more important in conditioning the thruster for proper operation. Without such conditioning, adsorbed gases from the electrode surfaces and organic-monolayers from the roughing and diffusion pump oil can significantly alter *both* the amount of mass in the discharge and the electrical conduction of the plasma near the electrode surface. Although these effects could indeed be beneficial to performance, *true performance* as would be expected in space operation, can only be measured after a conditioning period, and only as long as pump oil is not allowed to migrate to the thruster electrodes between discharges or test runs.

Three other pieces of evidence suggest that the performance measured at GE might include contamination effects:

1. GE's vacuum chamber used three 32" diffusion pumps that did not have baffles of any kind to prevent back-streaming. The closest pump was less than one meter away from the thrust stand [19].

2. Gridded ion velocity measurements taken by researchers at GE showed a significant amount of carbon and oxygen ions that varied from pulse-to-pulse. Although the total mass of these atoms may not have been significant compared to the xenon ions, their source and their effect on the current sheet structure remains unknown [27]. In addition, heavier molecules from pump oil can appear to have the same charge-to-mass ratio as xenon and be mis-interpreted as normal results.

3. General Dynamics constructed a very similar thruster to that of GE's A-7D and found, at best, a factor of two *smaller* performance [17].

That last item can best be visualized graphically with the results from Tables 3 and 6 being plotted in Figure 8. From this graph, it is easy to see that the data measured at General Dynamics has significantly lower performance than that measured at General Electric. It should be noted that General Dynamics and General Electric were competitors, however, only General Dynamics took the effects of background contaminants into account [17]. After 1970, there are no more publications from GE on GFPPTs, however, research at GE began on ablative pulsed plasma thrusters in the late 1960's with LaRocca.

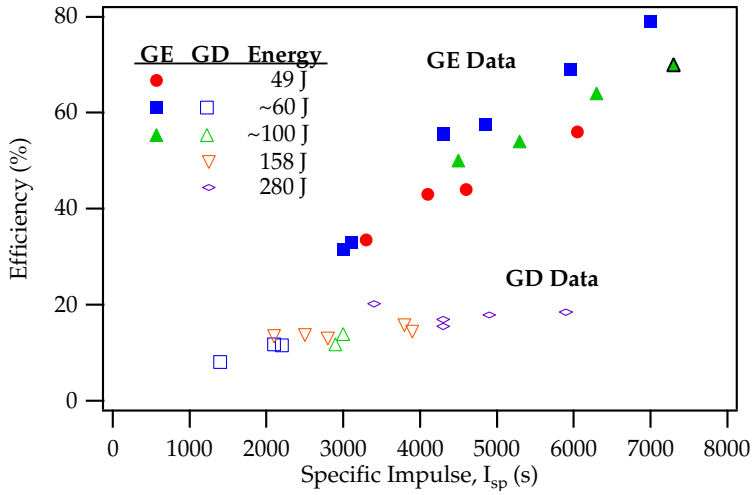

Figure 8: Graph of efficiency vs. specific impulse for the General Electric A-7D and General Dynamics A-7D replica GFPPT. Data taken from Ref. [17, 23] and also presented in Tables 3 and 6.

3 Lockheed

P.J. Hart. ***1962-1964***

Lockheed had a similar GFPPT development program compared to other labs. Thruster parametric studies along with computational models attempted to explain and predict GFPPT performance. In his first paper, Hart used a complete circuit model including a constant plasma resistance term and the normal snowplow mass accumulation model to predict the performance of three different accelerator designs. The first two, models A and B, tested the effects of initial inductance, while the third model C tested the effects of capacitance, however, unfortunately, other parameters such as the electrode geometry and energy were also changed simultaneously. In these accelerators, the outer electrode was actually made of a copper screen material to allow light from the

discharge to reach the rotating mirror of a streak camera. Table 7 shows the characteristics of the various designs.

Model	r_{inner} (cm)	r_{outer} (cm)	length (cm)	Init. Ind. (nH)	Capacitance (μF)	Energy (kJ)
A	0.64	2.38	7.0	90	2.0	1
B	0.64	2.38	7.0	240	2.2	1
C	0.74	7.40	84.0	150	300	15

Table 7: Lockheed accelerator designs. Taken from Ref. [28].

These parameters were inserted into his circuit-snowplow model and the resulting current sheet trajectory was compared to experimental measurements of sheet speed with streak photographs. In the model, the circuit and momentum equations were integrated until the velocity of the sheet began to slow down or asymptote. Test results using both hydrogen and air showed general agreement with the slope of the light trial (indicating the sheet velocity) front from streak photographs. Subsequent sheets, due to the oscillatory nature of the current waveform, were generally seen to travel *faster* than the first sheet. The measurements of sheet speed agreed relatively well with the snowplow model at high mass bits (the sheet moved slightly faster than predicted at the highest mass bit values) and fell well under the predicted speed at low mass bits, especially in tests with air. Hart believed this was due to the addition of back-plate insulator material (Teflon) to the discharge having more of an effect at low mass bits. Hart used Teflon because he found it to be the only insulator that provided a uniform, symmetric breakdown near the backplate.

Reducing the inductance and increasing the capacitance both seemed to increase the sheet speed, however, Hart did not believe this trend would continue indefinitely. He measured sheet speeds in the A and B configuration to see that the efficiency of B was nearly half that of A with the corresponding initial inductance gain of 2.7 times. Comparing relatively similar mass loading conditions in the C design, the increase in capacitance, initial inductance, inductance-per-unit-length, and energy led to a five fold increase in sheet speed. He also saw that the subsequent sheets were forming slightly *before* the current zero-crossings, possibly due to inductive effects. Magnetic probe data showed that "loop currents" were forming between each subsequent discharge.

Hart saw some polarity effects at low mass bits. With a positive polarity (anode at center) he saw a fainter, but faster, sheet that was overtaken by another, stronger sheet, possibly from the next current reversal cycle. He dubbed this as "Mode II" operation and thought that it would be preferable for thrusters to work in this way. Unfortunately, it is impossible to distinguish whether the current sheet is canted from streak photos which only show the first front of luminosity on either the anode or the cathode. Mode I operation (higher mass bits) did not show any polarity effects.

Slug-like mass distributions were used in the circuit model although they

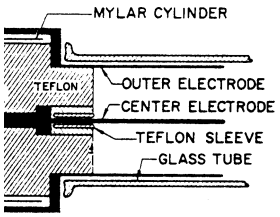

Figure 9: Schematic of Lockheed GFPPT with large radius ratio and Teflon backplate. Taken from Ref. [29] and modified to remove extraneous information on distributed inductance and physical discharge switch.

could not be realized in the experimental accelerators. Hart showed, as expected, that not as much energy goes into internal modes of the plasma for slug-like distributions with the predicted efficiency correspondingly higher. Current waveforms predicted from this slug-model were close to critically damped in character indicating a large rate of inductance change which, in reality, would require long electrodes. Hart also showed that the snowplow model could be modified slightly to account for the finite thickness of the current sheet although it did not significantly effect the results unless the thickness was on the same order as the thruster electrode length.

In later work, Hart tried many different electrode geometries varying primarily the inductance-per-unit-length by changing the radius ratio in coaxial thrusters [29]. Figure 9 shows a very high radius ratio thruster tested at Lockheed. Again, he used ambient filled thrusters with Teflon backplates and screen-like outer electrodes to permit optical access for streak photography. The capacitance was set to the lower value of the designs tested perviously, 2 μF, and the initial inductance was further reduced to 48 nH. In these thrusters, the discharge initiation was more stable and symmetric at the lowest gas pressures and smallest inner electrode radius values corresponding to the most ablated mass from the insulator. He also found that the snowplow model over-predicted the performance of the 1" inner electrode case and under-predicted the performance of the 0.063" inner electrode case (more exposed Teflon). He then presented a modified snowplow model that relied on only the force near the center electrode to determine the sheet velocity. This modified model agreed well with the data, however, it did not take into account the effects of insulator ablation.

3.1 Discussion of Research at Lockheed

Hart may have been the first one to realize that a solid-propellant Teflon thruster could have space-flight applications (see footnote in Ref. [29]). Although he tested a variety of geometries, capacitance, inductance, and mass bit values, unfortunately all of his experiments were influenced by the ablation of a significant amount of Teflon from the backplate. With gas propellant mass bits

between 10 and 500 μg and discharge energy levels being a 1 kJ or higher, The majority of the discharge could easily have been made up of Teflon at the lowest, middle, and even highest mass bits for the small inner electrodes. Although his computation models are valid (except possibly the modified form of the snowplow model), the results from streak photos that do not distinguish the *radial* position of the current sheet and should not be used as the only diagnostic for these potentially canted sheet. Unfortunately, these results with the Teflon contribution do not provide an adequate comparison or verification of the models that do not include its contribution. The "Mode II" operation showing the fastest sheet speed is probably a result of a very canted current sheet leading down the center electrode (anode) much faster than the true plasma center-of-mass.

4 Republic Aviation

L. Aronowitz, P.B. Carstensen, D.P. Duclos, F.P. Fessenden, W.J. Guman, P.M. Mostov, J.L. Neuringer, D.S. Rigney, and W. Truglio. ***1961-1964***

Research at Republic Aviation (more commonly know later as Fairchild-Republic for their later ablative pulsed plasma thruster work) began with a theoretical paper on the acceleration of a plasma slug [30]. They used a non-dimensional, constant mass model for the propellant eliminating any dynamic efficiency effects. They did not include any effects of plasma resistance, wall effects or radiation, although they did include a linearly distributed resistance for the electrodes. They tested two cases depending on integration time, however, they did not require a computer to solve the equations. Their "long time" model used asymptotic analysis to integrate the circuit and momentum equations out to an effective infinite time after the discharge. As any solution to the these equations shows a damped current waveform, the current flowing through will be zero and the velocity will be constant as time goes to infinity. Using this technique, the energy stored in the magnetic field and capacitor are always zero by the end of the integration. Along with the simple slug-mass assumption and without including the plasma resistance (instead, using a *constant* electrode resistance), the equations were solved at t=∞. The solution given for the efficiency is,

$$\eta(t=\infty) = 1 - \frac{2}{1+\sqrt{1+EL'^2/2m_{bit}R_0^2}}, \tag{8}$$

where $L^{'}$ is the inductance-per-unit-length, E is the energy per pulse, m_bit is the slug-mass accelerated, and R_0 is the constant resistance of the electrodes. In another solution case, the "short time" model assumed that the sheet motion was weekly coupled to the external circuit, i.e. that the inductance was *constant*. This assumption makes the problem linear with separate, analytic solutions to

the circuit and momentum equations. Again assuming a constant resistance,

$$\eta_{st} = \frac{1}{8} L'^2 \frac{E}{m_{bit}} \frac{1}{R_0^2} = \frac{1}{2\sqrt{2}} \frac{L'}{R_0} \bar{u}_e. \tag{9}$$

Including the effects of linear electrode resistance introduces a small correction and gives a cut-off for the initial inductance value where efficiency actually begins to slowly *decrease* for decreasing initial inductance,

$$L_0 \leq \frac{R_0^2 C}{9}. \tag{10}$$

Otherwise, interestingly enough, the initial inductance *does not* enter into the efficiency solutions at all.

Researchers at Republic first ventured into the experimental realm of pulsed plasma acceleration with a z-pinch, coaxial hybrid thruster shown in a cut-away side view in Figure 10 [31]. The average turn radius on the outer electrode is about four inches with the initial break-down occurring at the minimum inductance point, near the outer insulator walls. The thruster was designed so that as the current progressed, the stronger Lorentz force near the center electrode would help turn the current sheet to follow the electrodes. Propellant, in most cases nitrogen, was injected radially outward toward the outer insulator walls with the initiation occurring at the paschen breakdown point. At voltages below 2 kV this method of initiation did not always produce symmetric discharges. Therefore, typically 3 kV was used with a 120 μF capacitor bank (540 J) to produce a uniform current sheet. Maximum current in this device was 235 kA reached in about 1.3 μs indicating an initial inductance of about 20 nH. Typically the discharge volume was filled with 10^{14} cm^{-3} molecules of nitrogen before breakdown.

Photo-detectors, electric probes, and microwave interferometry all detected, with fairly good agreement (within 0.4 μs), the arrival of a plasma front traveling at about 90,000 m/s. The measured plasma density, however, was only on the order of 10^{14} cm^{-3} indicating that a small fraction of the nitrogen was not swept up in the current sheet or was left behind as neutrals recombined on the electrode walls. Still, the speed of this sheet was observed to be linearly proportional to energy, a result predicted by electromagnetic acceleration. The plasma conductivity was also seen to increase with increasing voltage from the interferometry measurements. Later measurements on the same thruster showed that this plasma front was close to perpendicular all along the electrodes although the sheet itself was spreading out as it propagated [32]. Also, a variety of different propellant types (hydrogen, helium, nitrogen, freon) were tried and photocell measurements showed a slight increase in velocity for smaller molecular weights, although all the velocities were relatively similar except in the extreme case of hydrogen.

William Guman joined the group in 1964 and began thrust measurements using a swinging-gate type thrust-stand that could measure the impulse from individual discharges. He found that regardless of propellant type, electrode

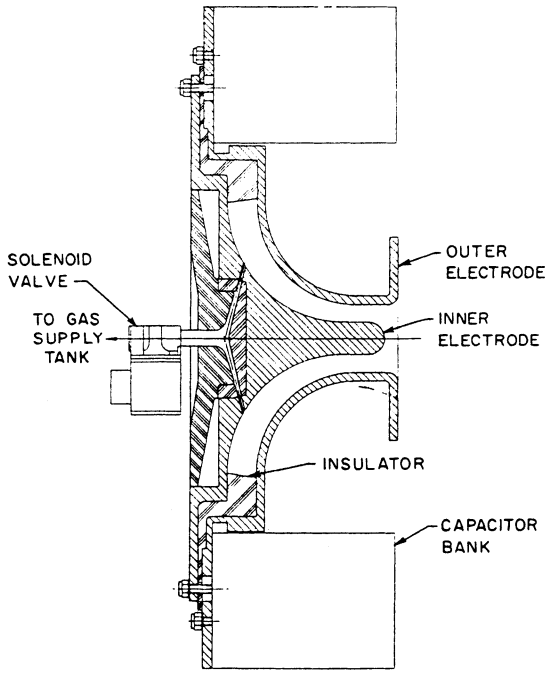

Figure 10: Schematic of Republic Aviation GFPPT with z-pinch, coaxial hybrid geometry. Taken from Ref. [32].

material, or background tank pressure (up to 10^{-4}) there was a decay in the measured impulse bit as the total number of pulses since the last facility pump-down accumulated [4]. Tests using a sealed thruster showed that most of this loss in impulse came from the subsequent loss of adsorbed gases obtained on the electrode surface when they were exposed to atmosphere. He also suggested that organic-monolayers from pump-oil contaminants could play a role, although noticeably smaller, in the decay phenomenon as well. Guman also showed that any erosion rate experiments need to include outgassing effects for accurate results.

In the final work at Republic, the delay due to the pulsed-gas and paschen breakdown type of discharge initiation was seen to lead to significant losses in propellant utilization [33]. If the breakdown did not occur quickly enough, propellant would leak out of the thruster electrode volume. If it occurred too quickly, not all of the propellant would make it out into the discharge volume before the breakdown. Guman fixed this problem by adding a gas-discharge switch in series with the accelerator that could be properly timed with the propellant flow [34]. Still, even with the subsequent propellant utilization efficiency improvement, it appears that switch lifetime issues and performance concerns drove Republic Aviation towards a different type of pulsed plasma accelerator, the Teflon ablative pulsed plasma thruster.

4.1 Discussion of Research at Republic Aviation

The non-dimensional slug model for acceleration presented in Ref. [30] is interesting in that it provides a resistance that varies as the current sheet moves down the electrodes, however, they found this to be a minimal effect. Their "short time" solutions do not include the effective resistance generated by the current sheet motion. Although this uncoupled model does not represent the electromechanical system correctly, it does provide a basis for understanding the performance scaling. Their "long time" solution includes the effects of changing inductance, however, it does not include the effects of subsequent discharges typically found in accelerators with an oscillatory current. It also does not take into account the finite length of electrodes and corresponding maximum change in inductance for a given geometry. Still, with all of these assumptions in mind, it does produce an interesting scaling relation for a slug-like mass, Eq. 8, that with Eq. 9, shows a monotonic increase in efficiency with increases in inductance-per-unit-length and energy, and decreases in mass bit and external resistance.

Unfortunately, the experimental work with the z-pinch coaxial hybrid thruster never produced an efficiency calculation in the journal publications. They were suggested to be below 50% from calculations of the amount of energy going into the internal losses of the capacitors [32]. Velocity measurements from probes do not necessarily correspond to the mass averaged exhaust velocity, however, as the sweeping efficiency of the sheet may not be 100%. For this thruster geometry, probably the most difficult thing to calculate was the mass bit which could explain the lack of efficiency data. In the summary produced by NASA

Lewis [2], efficiencies were shown to be around 14% at 3,000 s (9.5 μN/W) with nitrogen although the exact configuration of the thruster is unclear compared to the thruster found in journal publications. In his last paper, Guman did measure the thrust-to-power ratio (without specific impulse) and found that it asymptotes to about 9 μN/W at small mass loadings (previously tested conditions) and reached almost an order of magnitude higher, 80 μN/W at higher mass distributions. This was, by far, the largest thrust-to-power ratio measured for any GFPPT at the time, although the efficiency and specific impulse at this condition were probably very low. Still, the lack of continuing research on them at Republic after this measurement is puzzling, although Guman did begin ablative pulsed plasma thruster research soon afterwards.

5 NASA Lewis (now NASA Glenn)

S. Domitz, J.E. Heighway, A.E. Johansen, H.G. Kosmahl, C.J. Michels, P. Ramins, N.J. Stevens, and D.J. Vargo. ***1962-1965***

Researchers at NASA Lewis began studying plasma guns soon after Marshal (see Ref. [6]) showed that such a device could be useful for propulsion [35]. The coaxial accelerator at Lewis used propellant injection and an ignitron switch to initiate the discharge. The device itself, "Gun A," had an $r_{outer} = 4.75$ cm, $r_{inner} = 1.6$ cm (a radius ratio of about three), and a length of 48 cm, as shown in Figure 11. The first 9 cm length of the outer electrode (anode) was Vycor insulator with the propellant injection holes located 18.3 cm from the backplate. The capacitor bank was made up of eleven 1.1 μF capacitors charged up to between 10-30 kV (605-5450 J). The bank alone had a measured initial inductance of 10 nH although the initial slope from current traces predict a value closer to 70 nH which includes the cabling between the capacitors and the accelerator as well the inductance in the accelerator geometry itself. The propellant (hydrogen, nitrogen, or argon) was injected through a fast solenoid valve (100 μs) at various pressures to fill the chamber volume near the propellant injection holes with a 1.1 ms delay between the valve actuation and the ignitron switch closing. The discharge was reported to initiate near the propellant injection holes, and not near the backplate. Faster injection times giving more slug-like mass distributions were later seen to be subject to "spoking instabilities" in Ref. [36].

In these devices, the sheet speed was determined by a series of magnetic probes along the accelerator's outer electrode. The efficiency was calculated using a combination ballistic pendulum-calorimeter to measure the final plasma kinetic energy. Heading Guman's observation of impulse decay [4], ten pulses were fired before any measurements were taken to "outgas" the electrodes. They found the sheet velocity from magnetic probe data to asymptote to a value that was independent of propellant density although there was a weak dependence on molecular weight ($V_{H_2} = 160$ km/s, $V_{Ar} = 100$ km/s). This velocity was measured after a crow-bar discharge occurred near the backplate, approximately 1.5 μs after initiation and in coincidence with the *voltage* reversal or maximum

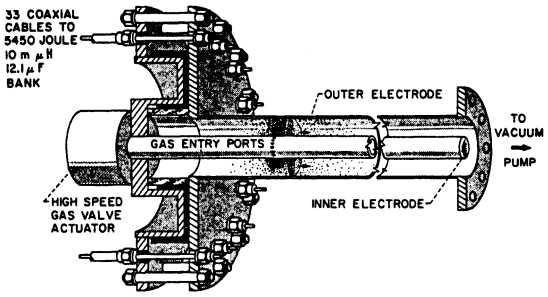

Figure 11: Schematic of NASA Lewis "Gun A" GFPPT. Taken from Ref. [35].

current. The ballistic pendulum-calorimeter measurements showed that argon had the best overall efficiency, 12%, which peaked at about 100 μg of propellant. Hydrogen reached its peak efficiency at a lower mass bit, 10 μg, with a value of 9%. In general, the efficiency was seen to scale with the square root of the energy to mass bit ratio.

These performance measurements along with others testing variations in propellant injection location were later compared to a fairly complete, non-dimensional snowplow model [36]. This model originated from previous work described in Ref. [37]) that used a slug-mass for the injected propellant and the snowplow effect for mass that was eroded from the electrodes and accumulated as the current sheet progressed. As can be expected, the performance in this first model strongly depended on a mass ablation coefficient that determined the ratio of ablated electrode mass to injected propellant mass. The overall trends, however, showed a similar global result to other one-dimensional models with the highest predicted performance corresponding to large values of inductance-per-unit-length, initial voltage, capacitance and small values of initial inductance and resistance.

The more advanced, non-dimensional model presented later in Ref. [36] used a distributed propellant mass and included terms for ionization energy losses, radiation losses, wall drag due to ion diffusion, and heat transfer from the plasma to the electrodes through the inclusion of a plasma energy equation[4]. Comparing results from a simplified model that did not include these effects showed that they consumed no more than 33% of the initial capacitor energy, with smaller discrepancies (less relative loss) at *higher* energies (see Fig. 12). Both families of solutions had a similar dependence on the mass profile with the highest performance predicted for more slug-like distributions. The simplified model also examined the effects of crow-baring at a beneficial time when the current is zero (no energy is stored in the magnetic fields) and at the worst time when the current is maximum. In general, the effects of choosing an appropriate crow-barring time were more pronounced than those observed from the addition of the various

[4]Please see the following discussion sub-section for a more detailed description on how these terms were handled.

loss mechanisms with up to a 40% performance reduction predicted using the "maximum current" crow-bar time. Experimentally, the crow-bar time was seen to depend on accelerator geometry, especially near the breech. Later geometries included an "inhibitor ring" that delayed the crow-bar to when the total current was beyond the maximum value. The performance measurements are presented in more detail in the next section, however, in general, they did not match the predictions in either absolute values or functional form. The author's explain this discrepancy is based mainly on the incorrectly modeled initial mass density profiles.

Research on *unsteady* pulsed plasma thrusters at Lewis stopped in 1965 after it was observed that the current sheet stabilized at the end of the accelerator after 12 μs [38] leading to further "quasi-steady" research. Also in 1965, Researchers at Lewis outside of the experimental group produced a comprehensive review of GFPPT research at many laboratories which brought out the following points [2]:

1. Calorimetry data from many labs did not agree with the subsequent performance data measured on thrust-stands. Thrust-stand data was generally accepted as the most accurate way to measure performance.

2. Crow-baring generally occurs in all unsteady devices sometime between the voltage and current reversal points depending on thruster geometry and driving circuit parameters.

3. The main acceleration mechanism inside the current sheet was believed to be primarily due to the polarization field created by the electrons trapped on an $E \times B$ drift and the subsequent charge separation. The report also mentioned, however, that many of the labs had very different results and disagreed in this area, especially on the influence and existence of ion conduction.

4. The coaxial geometry (compared to pinch or parallel-plate) was suggested to be the best because it trapped all of the electromagnetic fields although it has a large electrode surface area and small inductance-per-unit length which decreased efficiency.

5. Including an electric switch in the discharge initiation process (as apposed to using the Paschen break-down point alone) led to better repeatability, fewer spoking instabilities, and improved propellant utilization while, at the same time, it introduced parasitic inductance and resistance as well as adding reliability questions.

6. The report's conclusion stated the need for a simple performance model that was confirmed by repetitive, experimental performance measurements.

7. The report also stated that the only thing keeping GFPPTs from being used in space was their lack of "heat handling capability" and that research was shifting to quasi-steady devices which might have better performance.

5.1 Summary of NASA Lewis Performance Measurements

Researchers at NASA Lewis measured the performance (calorimetry) of four different accelerator designs, as shown in Table 8 and taken from Ref. [36]. The thruster was conditioned by firing ten times prior to any measurement. All the designs used mainly argon for propellant and an ignitron switch for discharge initiation timing. The propellant utilization for these devices was estimated to be 100% due to the short valve times (0.1 ms) and long gun barrels. The accelerators were all backed by a 12.1 μF capacitor bank that could be charged up to as much as 30 kV. Reduction in parasitic inductance came from improving the connection between the capacitor bank and accelerator as well as modifications to the gun geometry itself. Even with changes in propellant injection location, initial inductance, and inductance-per-unit-length, no noticeable difference in performance was measured until the electrode length was reduced by slightly more than 50%. Unfortunately, the inductance-per-unit-length was also changed in this configuration making the correlation with the stronger Lorentz force or reduced wall losses difficult to differentiate.

Gun	r_{inner} (cm)	r_{outer} (cm)	length (cm)	Prop. Inject. Location (cm)	Init. Ind. (nH)	Max. Eff. (%)
A	1.6	4.75	48	18	80	12
B	1.6	4.75	46	2	44	13
C	0.64	4.75	46	2	23	13
D	0.32	4.75	20	2	23	22

Table 8: NASA Lewis accelerator characteristics. The maximum efficiency point is from calorimetry measurements using argon at close to 4000 J (25 kV) over a range of three to four mass bit values. Taken from Ref. [36].

5.2 Discussion of Research at NASA Lewis

Probably the two biggest contributions from NASA Lewis are the most inclusive acceleration model published from any of the labs [36] and the review of GF-PPT research in 1965 [2]. Performance measurements at Lewis did not include thrust-stand data, although the thruster was pre-conditioned to eliminate electrode contamination. In addition, although changes were made in thruster geometry, propellant distribution, and energy, they were not systematically tested so correlation between the modifications and performance improvements could only be speculated. Finally, with only a few mass bit values tested and no amount of error reported, the trends presented in the data are difficult to draw conclusions from.

Non-Dimensional Snowplow Model. NASA Lewis developed an acceleration model that included the effects of a variable mass distribution (from slug-

like to uniform), and losses from "wall drag", heat transfer, ionization, and radiation [37, 36]. The exact details are left to the cited publication, however, the most important points are summarized here:

- The mass distribution function is not related to any physical phenomenon; that is, it does not have an exponential or linear nature that would be expected from pulsed gas injection or a uniform fill.
- Wall drag includes the loss in forward momentum from ions diffusing to the wall based solely on temperature and not current conduction.
- The internal energy of the plasma is based solely on temperature without including pressure effects. Energy is transferred to the plasma from the mass accumulation process and ohmic heating. Energy is lost from the plasma through heat conduction to the electrodes, electron current conduction, ion diffusion and recombination near the electrodes, ionization and radiation. It should be noted (by the author's own admission), however, that although ohmic heating, ionization, and radiation losses appear in the equations, they are not included in the actual solutions.
- The initial temperature is not specified explicitly in Ref. [36] and no profiles for plasma temperature are mentioned or displayed.

The effects of introducing the plasma energy equation are present in comparing the results of the more advanced model with one that does not include these losses, as shown in Figure 12. In general, the efficiency is found to follow a similar trend, peaking at a particular "Mass Loading Parameter" that is slightly smaller than what is predicted by the simplified model. The relative loss is smallest at small values of the Mass Loading Parameter. The Mass Loading Parameter is defined as,

$$\mathcal{M} \equiv \frac{2\ell m_0}{L' Q_0^2} = \frac{\ell m_0}{L' C E_0} \tag{11}$$

which includes the amount of mass in the initial discharge (m_0), the initial energy (E_0) or charge (Q_0) on the capacitor, the capacitance (C), the inductance-per-unit-length ($L^{'}$), and the length of the electrodes (ℓ), but *not how the mass is distributed*. This definition makes it hard to differentiate between the various parameters, and its experimental value strongly depends on the initial mass taken up by the current sheet, a very difficult quantity to determine. The authors suggest that the largest loss is through ion diffusion to the walls and that radiation losses are negligible, although they do not provide magnitudes, relative or absolute. They also suggest that radiation cooling could play a significant role, although it is not included in the final plasma energy equation. Although the model did not seem to match well with experimental data, this could have been as much a result of trusting calorimetry performance data then the fault of the model. Without more information on the temperature profile as a function of time, it is hard to say if the plasma energy equation and the associated

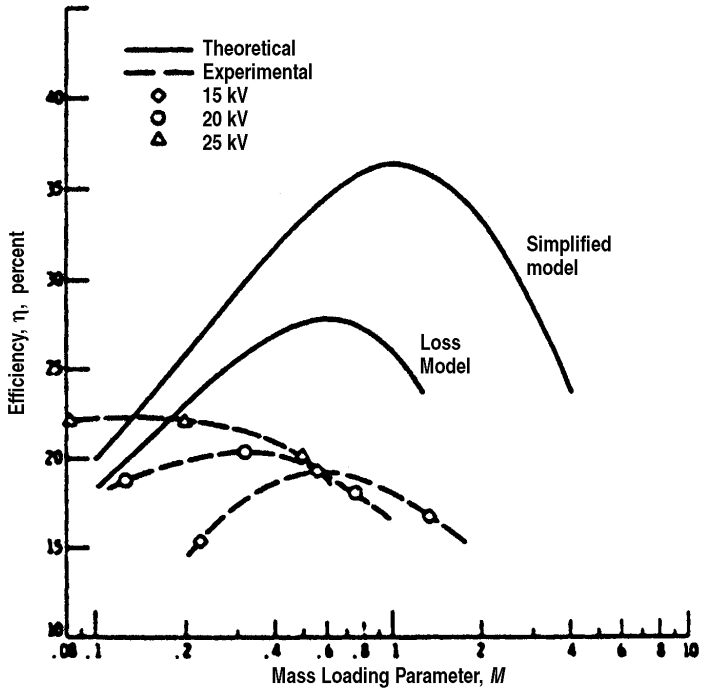

Figure 12: Graph of Efficiency vs. Mass Loading Parameter (see Eq. 11) including theoretical curves (both simple and advanced) and measured performance data (calorimetry) from "Gun D" using argon at 15, 20, and 25 kV. Taken from Ref. [32].

assumptions were reasonable. Finally, it should be noted that the advanced model did not take crow-baring into account and used a non-dimensionalization scheme based on the *final* inductance of the current sheet at the end of the electrodes, assuming it got there before the current reversed and a crow-bar discharge was formed. The integration was carried out until the current sheet reached the end of the electrodes.

GFPPT Review. The GFPPT review in Ref. [2] provides a very important picture in continuing GFPPT development. Besides presenting a research summary shown in the itemized list of the previous section, it begins to explain why GFPPT research was not pursued much past 1966 in any laboratory at the time besides Princeton. With most efficiencies being below 50% and the reliability of the electrical switches and fast-acting valves in question, research shifted to higher performance quasi-steady pulsed plasma accelerators for main propulsion applications, and the simpler ablative pulsed plasma thruster for attitude control applications. Until only recently, as described in the next section on research at Princeton, have GFPPTs resurfaced as an alternative electric propulsion device once again, this time at lower energy (< 10 J).

6 Princeton

N.A. Black, R.L. Burton, E.Y. Choueiri, K.E. Clark, E.A. Cubbin, A.C. Eckbreth, W.R. Ellis, R.G. Jahn, W. von Jaskowsky, T.E. Markusic, P.J. Wilbur, T.M. York, J.K. Ziemer, and D. Birx (SRL Inc.). ***1962-present***

The research at Princeton on unsteady electromagnetic acceleration can be divided in two categories based on research period, apparatus, and type of investigation. From 1962 until 1970, the structure of the current sheet in a z-pinch was examined including Kerr-cell photos, magnetic and electric field surveys, fast-response pressure probe measurements, and microwave interferometry. In 1969, Jahn wrote "Physics of Electric Propulsion" (Ref. [1]) which included a summary of GFPPT work up to that point. From 1970 until about 1997, Princeton focused on quasi-steady and steady-state MPD thrusters as well as some work dealing with ablative pulsed plasma thrusters in the 1990's. After 1997, in cooperation with Science Research Labs (SRL) Inc., GFPPT research began again focusing mainly on improving the performance of low-energy (< 10 J), low-mass versions of the coaxial guns of the past. In addition, a new study of unsteady current sheet canting and stability began in 1999. As this part of the review includes work by this author, there will be no discussion subsection, rather, the work at Princeton is divided into two separate subsections based on topic.

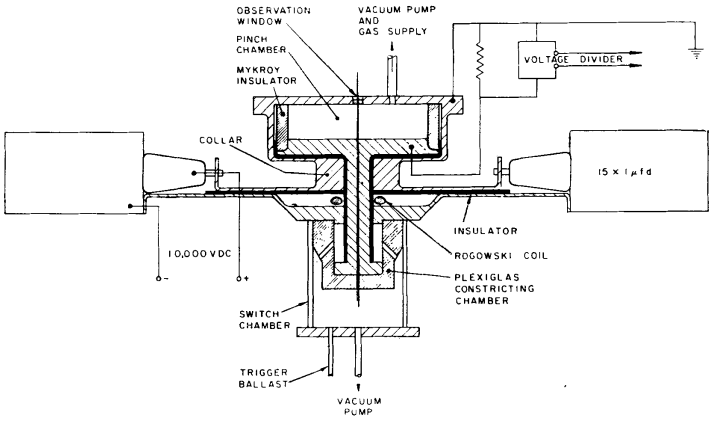

Figure 13: Drawing of Princeton Z-Pinch Apparatus. Taken from Ref. [39].

6.1 Basic Acceleration Scaling Studies at Princeton

Basic acceleration scaling studies began at Princeton in 1962 using a pre-filled z-pinch with a large outer radius [39] and investigating the basic scaling properties of the device. This device was used extensively in many of the studies and has the following dimensions: r_{outer} = 10.2 cm, electrode gap = 5 cm, as shown in Figure 13. Fifteen 1 μF capacitors were connected in parallel around the circumference of the device and charged up to 10 kV (750 J) yielding a damped oscillatory waveform with a peak current of 200 kA. The peak current was reached in 0.4 μs after the activation of a gas-switch indicating an initial inductance of about 20 nH [40]. Argon was used for propellant with an ambient pressure of between 20 mT-10 T before the pulse. Optical measurements from streak-photographs showed that the sheet velocity depended on the inverse of the square-root of the density. From magnetic field measurements it was found that a bulk of the current was actually carried near the outside insulator, near the initiation point, soon after the first sheet moved slightly inward. In time, the formation of the second sheet corresponded to the maximum voltage, or current zero-crossing. Internal current loops between the two sheets were found that maintained the same current *direction* in the first sheet. These circulating currents did not appear to be conducted through the electrodes allowing a 7.6 cm radius circle to be cut out of the top electrode and replaced by a pyrex window. Kerr-cell photographs showed that the sheet broke down near the outer insulator uniformly and propagated inward without instability and with no effect seen from the pyrex window. A C-channel like pyrex insert was used to examine the initial breakdown. It was found that although the current sheet still formed near the lowest inductance points at the electrodes, it remained planer and did not bend outward along the inner surface of the channel. Once again, it propagated uniformly inward indicating that the magnetic effects were greater than the gas

dynamic effects.

Studies continued on this device with more magnetic field measurements and the development of a snowplow model for z-pinches based on Rosenbluth's work at Los Alamos (see Ref. [41]). It was found that the luminous front fell slightly behind the current conduction zone of the first current sheet until the second sheet formed and subsequently conducted most of the current. It was also found the both the luminous front and the current conduction zone were traveling *faster* than what was predicted based on a snowplow model. It was concluded that the current sheet formed with the $r_{outer} = 10.2$ cm geometry was permeable with less than a 100 % sweeping efficiency. Inserting an insulating ring at $r = 5.1$ cm was shown to increase the sweeping efficiency to 100 % with the luminous front, current conduction zone, and snowplow model trajectory all in close agreement. The sweeping efficiency was also found to increase with increasing energy and decreasing mass bit. When the sweeping efficiency was high, the sheet velocity was seen to scale as expected with the non-dimensional "magnetic interaction parameter" β,

$$\beta \equiv -\frac{\mu_0 Q_0^2}{4\pi^2 \rho_0 r_0^4} = -\frac{\mu_0}{2\pi}\frac{h}{r_0^2}\frac{CE}{m_{bit}}, \tag{12}$$

where ρ_0 is the initial density, r_0 is the outer electrode radius, and h is the distance between the electrodes. Various values of the β parameter were investigated using different mass densities and outer electrode radii. The pinching effect was also found to be a strong function of β with the pinch occurring *before* the current reversal for tests with $|\beta| > 0.2$.

Research then turned to channeling the radially directed sheet into axial momentum. First, Jahn and Black showed that the z-pinch is an inherently good device for dynamic efficiency concerns as most of the propellant mass is swept up in the beginning of the discharge. In Ref. [42], he laid out how the overall efficiency could be greater than 50% as long as the propellant mass was swept up when the current sheet velocity was small. Next, Jahn and Burton built a 15.24 cm diameter, 61 cm long vacuum chamber around the top electrode of the z-pinch and removed the pyrex window to allow the plasma to expand outward from the pinch [43]. The electrode configuration was slightly changed for this device to reduce the parasitic inductance further and improve the sweeping efficiency with an inner radius of 6.35 cm. The peak current was close to 300,000 A with the same 15 μF, 10 kV capacitor bank. The entire volume (including the new exhaust chamber) was filled with argon propellant between 30-1920 mT before the discharge. Various exit orifices were tested (0.95, 1.9, 3.8, 5.1, 7.6, and 10.2 cm diameter holes cut in the center of the top electrode) and it was found that the luminous front expanded with a speed that increased with increasing diameter until the 10.2 cm case. In that case, only a little over 1 cm of electrode was left near the outer insulator, possibly not providing enough electrode surface area for proper conduction. It was also found that the expanding axial front traveled with a little over half of the original inward radial sheet velocity until, eventually, the core of the pinched plasma caught up and passed the front. The best case of radial velocity change to axial velocity came

for the 120 mT case where the ratio of the two velocities was near 80%. Again, current probe measurements showed that the sheet moved radially inward in a very similar fashion to the set-up with the pyrex window, and that the luminous front corresponded well to the beginning of the current conduction front.

In more recent work at Princeton, two models for performance scaling have been developed for coaxial and parallel-plate electrode geometries: a simple, fixed element approximation [44], and a full, single axis, non-dimensional model including the effects of a flared electrode geometry and an exponential mass distribution [45]. In the fixed element solution, primarily modeling a critically damped waveform, the inductance was assumed not to change (although it was given an *average* value, $< L >$, greater than the initial inductance, L_0), and the effective resistance was also held constant. The impulse was assumed to depend solely of the integral of the current squared with the final relation showing a linear dependence on the initial energy stored in the capacitor,

$$I_{bit} = L^{'} \sqrt{\frac{C}{< L >}} E. \tag{13}$$

The efficiency was predicted as,

$$\eta = \frac{I_{bit}^2}{2 m_{bit} E} = \frac{1}{2} L^{'2} \frac{C}{< L >} \frac{E}{m_{bit}} = \frac{1}{2} L^{'} \sqrt{\frac{C}{< L >}} \bar{u}_e. \tag{14}$$

Note that in this approximation, the average inductance quantity depends on the position of the current sheet and the inductance-per-unit-length. In this way, the efficiency could also be considered to depend on $\sqrt{L^{'}}/\sqrt{\ell_{elect}}$. In any case, both the impulse bit (thrust-to-power ratio) and the efficiency are expected to scale with a square-root of capacitance. In the more complete non-dimensional model, the performance was seen to behave differently depending on the nature of the current waveform. In general, the efficiency increased with decreasing circuit resistance, however, for the underdamped cases with a uniform propellant fill, a maximum in the efficiency was found with a Dynamic Impedance Parameter, α, value near unity,

$$\alpha = \frac{L^{'3} V_0^2 C^2}{18 L_0^2 m^{'}}, \tag{15}$$

where $m^{'}$ is the mass density gradient coefficient. For critically or overdamped cases with a uniform fill, the efficiency increased with $\alpha^{1/4}$ yielding,

$$\eta \propto \sqrt[4]{\frac{8 L^{'3} V_0^2}{9 R_0^4 m^{'}}}, \tag{16}$$

with R_0 (including only the internal capacitor resistance and the plasma resistance) having the strongest influence. The thrust-to-power ratio *decreased* with increasing α for the underdamped cases and remained relatively constant over α for the critically or overdamped cases. Using an exponential mass distribution increased the efficiency and thrust-to-power ratio in accordance with the dynamic efficiency improving. The character of the efficiency was also changed for

the underdamped case with the maximum point shifting to much higher values of α, > 10. Higher values of α, however, were also seen to require very long electrodes with total inductance changes on the order of $100 \times L_0$ which are very difficult to achieve in reality. The nature of the thrust-to-power ratio did not change for the exponential mass distribution. Using flared electrodes also improved performance, but not to the same extent as the non-uniform propellant density. Further development of this model including crow-baring for the underdamped cases and finite electrode effects are ongoing at Princeton.

6.2 Current Sheet Structure Studies at Princeton

Three PhD thesis [46, 47, 48] and three journal publications [49, 50, 51] by Burton, Ellis, and York, respectively, examined the structure of the current sheet through electric and magnetic field probing, microwave interferometry, and fast-response pressure measurement. These three sources will be combined (Note: Ref. [50] provides the best summary of the work as it is published after all the work had been completed) to form a coherent picture of current sheet structure as developed at Princeton. Although all of these measurements are taken at the midline of the z-pinch apparatus and at a radius half-way between the outer insulator and the center, there is no reason to think that a similar structure shouldn't exist in other pulsed accelerators with different geometries. The reader should consult all of these references for the entire story including the model development between references. Only the most simple, coherent results will be reproduced here.

First, the author's start with a generalized Ohm's Law in the frame of the moving current sheet (current sheet moves in *radial* direction in a z-pinch),

$$\vec{j} = \sigma_0 \left(\vec{E} + \vec{v}_i \times \vec{B} + \frac{\nabla P_e}{n_e e} \right) - \frac{\Omega_e}{|B|} \vec{j} \times \vec{B}. \tag{17}$$

where all the terms here have the familiar definitions. Note that the Hall conductivity for the electrons (but not the ions) was included because the chamber dimensions were assumed to be much larger than the electron gyro-radius, but smaller than the ion gyro-radius. Also, the effects of ion-slip were not included, and an assumption of complete, single ionization occurring as soon as the molecule enters the sheet was held throughout the publications. The electric and magnetic fields were measured with probes [49] while the scalar plasma conductivity, plasma temperature, and density were measured by microwave interferometry [50]. The Hall parameter was inferred from these measurements as was the electron pressure from the kinetic relation, $P_e = n_e k T_e$. Only the azimuthal magnetic field was found to be significant while, similarly, only the radial and axial components of the electric field were important. In the moving frame of the current sheet, the radial ion velocity is assumed to start at sheet speed (measured from streak and Kerr-cell photos as well as probe arrival time data) and slow to zero, eventually traveling with the current sheet. As the axial current density is known from total current measurements as well as magnetic

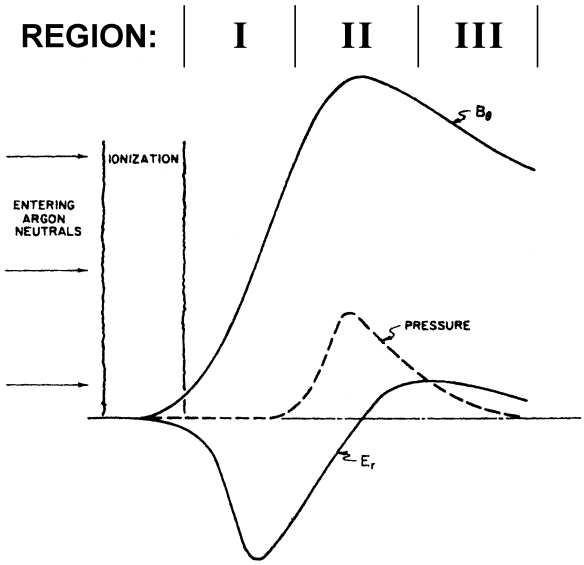

Figure 14: Radial electric field, azimuthal magnetic field, and heavy species pressure profiles in the current sheet frame. Taken from Ref. [49] with modifications to show regions identified in Refs. [50, 51]. The area of expected pressure increase was confirmed in Ref. [51]

field probe data, only two unknowns remain: the radial current and the axial ion velocity. Measurements of these parameters in the current sheet frame of reference are presented in Figure 14.

It should be noted that the axial electric field should be expected to be very nearly balanced by the back EMF of the moving current sheet so that the *axial* electric field actually dominates the conductivity. As seen from the measurements, this was found to be true with the appearance of three regions bounded by the character of the radial electric field. In Region I, the radial electric field is very large and caused by the separation of the electrons caught on an $E \times B$ drift while the ions have a large amount of momentum and penetrate deeper into the sheet. This radial electric field does, however, slow down the ions into Region II, although it emphis not enough to slow the ions down completely to sheet speed. Region I was found to be dominated by axial electron current making up a significant fraction of the total current, but *not* enough for the *entire* current. Region I was found to be about 5 mm thick for argon. As the separation of the ions and electrons induces a radial polarization field, it also creates a radial current. This radial current, although relatively small, interacts with the azimuthal field enough to cause the ion trajectories to deflect towards the cathode. In Region II, with the ions now moving slower and slightly deflected, *axial ion current* dominates with ions recombining on the electrode

surface to complete the total current. This produces a $j_{iz} \times B_\theta$ that further decelerates the ions to sheet speed. Region II was also found to be the location of a large heavy species pressure gradient. As the radial electric field actually reverses sign (although not to the same magnitude) in Region II, the electrons actually try to drift against the current flow, however, with the greater ion density, collisions dominate and they remain relatively stationary with respect to the sheet. In Region III, the axial electric field is still negative, although smaller and returning to zero. As the ion density is low here, there is actually the possibility of a small reverse current being carried by the electrons in the trailing edge of the current sheet. The total sheet was found to be about 1 cm thick at the center line with a slight tilt, anode front leading cathode.

This tilt or cant of the current sheet has been investigated in more recent work at Princeton in a parallel plate accelerator [52]. In brief, optical measurements of sheet speed and tilting angle have qualitatively found that larger molecular weight propellants experience more canting, and that the canting angle is independent of initial voltage or peak current. Research is continuing with Schlieren photography.

6.3 Performance Measurements of Low-Energy GFPPTs at Princeton

In 1997 Princeton's Electric Propulsion and Plasma Dynamics Laboratory (EPPDyL) began developing low-energy GFPPTs in cooperation with Science Research Laboratory, Inc. (SRL). The research focused on the following goals [53]:

1. Developing a low-mass (low-energy) GFPPT with the same or better performance as GFPPTs at higher energy. A target was set for 50% efficiency at 5000 s (thrust-to-power ratio of about 20 μN/W) based on the results from GE, but using only 1 J per pulse.

2. Designing a GFPPT that has a 100% mass utilization efficiency using existing, space-qualified valves that have greater than a one million cycle lifetime.

Achieving the these goal included:

- Using solid-state switching technology to increase pulses rates to above 4 kHz for high propellant utilization.

- Grouping pulses together in *bursts* to allow thrust and power modulation while also reducing the total number of valve cycles over the lifetime of the device.

- Developing a highly accurate ($<$ 10% error), low-impulse (($<$ 100μNs), thrust stand and high-speed current sheet visualization techniques.

- Rapid thruster prototyping to examine changes in geometry, propellant injection, discharge initiation, and driving circuit.

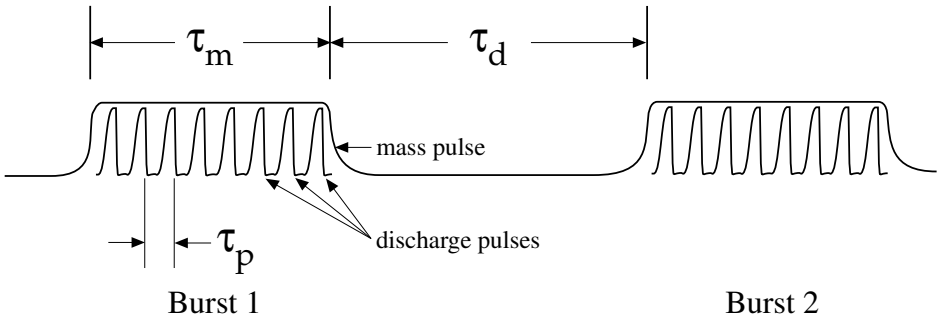

Figure 15: Schematic of a burst of pulses in an SRL-EPPDyL GFPPT.

- Creating a low-energy discharge initiation system that provides a reliable, uniform, symmetric current sheet without inducing a large amount of erosion.
- Deriving and testing performance scaling laws based on simple analytic and complex non-dimensional models for current sheet acceleration.

To date, nine generations of SRL-EPPDyL GFPPTs have been tested with many modifications on each generation. Using a low-voltage (250 V), low-inductance (< 5 nH) capacitor bank (45-270 μF, 1.4-8.4 J), these GFPPTs have close to critically-damped current waveforms with no noticeable crow-baring. Peak currents are close to 10 kA with pulses lasting about 5 μs. As shown schematically in Figure 15, during a burst the valve is only cycled once, therefore, the ultra-fast, high energy valves used in previous GFPPT designs are not required. As the propellant flows at a constant rate, the propellant utilization is dictated by the pulse frequency and the thermal velocity of the propellant. For example, using argon ($v_{th} \approx 400$ m/s) and a 4 kHz pulse frequency, the electrodes are required to be at least 10 cm long to ensure that none of the propellant escapes outside of the discharge volume between pulses.

Although many different GFPPT designs have been tested at EPPDyL, the fifth-generation (designated as PT5) has undergone the most extensive performance measurements. Since its original design, changes have been made to its discharge initiation system and propellant distribution [10] as well as the performance measurement technique to insure proper conditioning [5]. As shown in Fig. 16, PT5 uses a stainless-steel, coaxial electrode set with an outer to inner electrode radius ratio of approximately four and a total volume of 350 cm^3. It uses four semi-conductor type surface-flashover spark plugs mounted on the inside of the outer electrode (cathode) at 90 degree azimuthal intervals to initiate the discharge uniformly. The main discharge is driven by a low-inductance (10 nH) 130 or 270 μF capacitor bank which is capable of being charged to 250 V giving a maximum energy per pulse of 4 or 8 J, respectively. The entire thruster has a mass of approximately 6 or 8 kg depending on the

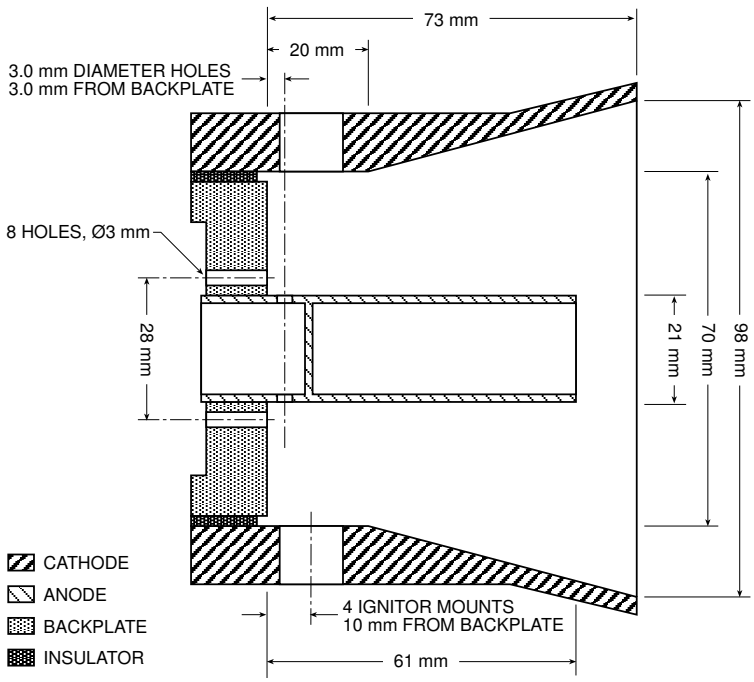

Figure 16: Schematic of SRL-EPPDyL PT5.

capacitance level and including the electrode mass as well as the thruster housing mass. High-speed photographs of the discharge were taken with an Imacon Fast-Framing Camera (IFFT) at rates of 500,000 frames per second. A series of IFFT frames of PT5 showing the symmetrical discharge initiation are presented in Fig. 17. Before the modifications to the gas manifold were made to make propellant injection more uniform, the discharge initiation was seen to occur near the region of highest pressure. This is a similar result to those researchers who found spoking instabilities when the discharge was allowed to initiate based solely on a Paschen breakdown without an external switch.

Two energy levels for each of two capacitance values were tested over ten different mass bit values each yielding a 40-point GFPPT performance database. Four graphs which show PT5 performance as a function of mass bit and specific impulse with the capacitance and the initial stored energy level as parameters are shown with error bars in Fig. 18. Each point represents at least twenty trials including separate measurements of impulse, mass bit, and energy at the same conditions. Values of the performance data are given at the end of this section in Table 9. It is evident from all the plots in Fig. 18 that for each curve there is a transition with decreasing mass bit (or increasing I_{sp}) from a mode (Mode I) where the efficiency and the impulse are respectively independent and dependent on the mass bit (and where the efficiency the thrust to power ratio

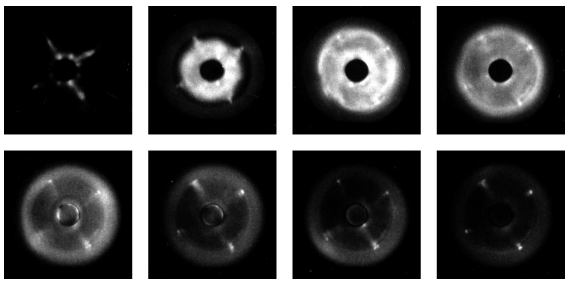

Figure 17: Unfiltered Imacon Fast-Framing Camera photos of a typical PT5 discharge looking straight into the discharge chamber using 0.5 μg argon and 4 J of energy per pulse. The photos seen here are spaced by 1 μs going from right to left and top-right to bottom-left.

are respectively independent and dependent on I_{sp}) to another mode (Mode II) where the converse statements hold.

Simple analytic models presented in the previous section show that the efficiency and thrust-to-power ratio should scale with the square-root of capacitance and not depend on the energy (at a constant exhaust velocity) for an electromagnetic accelerator. These trends are evident in Mode II where the efficiency increases linearly with the specific impulse and the thrust-to-power ratio is relatively constant.

It is interesting to note that the performance scaling suggested for a thruster where electrothermal acceleration is dominant are quite different[54]. In that case, the impulse bit is expected to scale with the square root of the discharge energy to mass bit ratio and not depend directly on capacitance or inductance change. In addition, the efficiency of a pure electrothermal accelerator is expected to be constant over wide range of specific impulse, energy and mass bit values. While the efficiency as seen in panels c and d of Fig. 18 is indeed independent of mass bit and I_{sp} at high mass bit values (i.e. Mode I), it does show a dependence on energy, albeit a weaker one than for Mode II. This tends to indicate that the acceleration in Mode I may be due to a combination of both electrothermal and electromagnetic effects. Again, as the losses associated with sweeping up the propellant are not accounted for in these predictions, an explanation for trends in Mode I could be a function of improved dynamic efficiency as well.

Later generations of SRL-EPPDyL GFPPTs were used to examine lifetime issues and inductance-per-unit length effects. PT7, a parallel-plate "quad" design (see Ref. [55]), was pulsed 1.5 million times at a discharge energy of 2 J with 0.3 μg of xenon propellant per shot. As seen in Figure 19, the single spark-plug initiation system used in this design was severely damaged with measured erosion rates of 0.2 μg per shot. Although the spark-plug did not short-out in this test as it did in a subsequent 100,000 pulse test, it is seen to be the

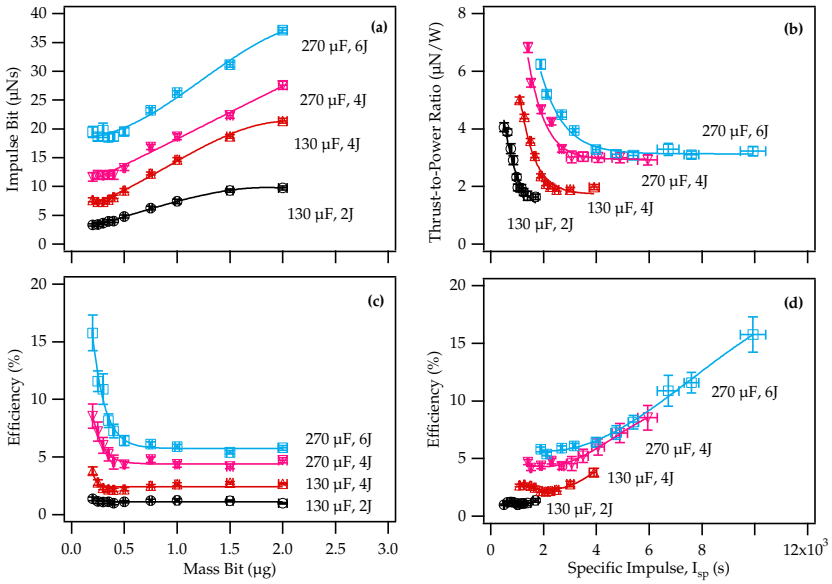

Figure 18: Performance of PT5. Graphs (a) and (c) show the impulse bit and efficiency as a function of mass bit. Graphs (b) and (d) show the thrust-to-power ratio and efficiency as a function of specific impulse. All graphs contain four curves which show changes in performance due to changing capacitance values and initial stored energy levels.

Figure 19: Cathode of SRL-EPPDyL PT7 showing the damage to the surface-flashover spark-plug after 1.5 million pulses.

lifetime limiting component of this GFPPT design. Later designs switched to a lower-energy RF spark-plug (PT8, see Ref. [56]) and an even smaller surface-flashover plug (PT9, see Ref. [57]) that did not have an electrode in common contact with the thruster electrodes. Erosion rates have now been measured to be below 0.1 μg per pulse in both systems, however, system mass and lifetime concerns still need to be addressed. The latest design, PT9, was also used to examine the effects of inductance-per-unit-length on performance although the pyrex side-walls used to contain the plasma in the parallel-plate geometry were suspected to induce a large amount drag on the current sheet, reducing performance [57]. More recent studies at EPPDyL include testing PT9 without sidewalls, and will be presented later this year.

Cap. (μF)	Energy (J)	m_{bit} (μg)	I_{bit} (μN-s)	I_{sp} (s)	η (%)
270	4.0	0.20	11.6	5940	8.53
		0.25	12.0	4890	7.20
		0.30	11.9	4060	6.01
		0.35	12.0	3500	5.22
		0.40	12.0	3060	4.56
		0.50	13.2	2680	4.35
		0.75	16.9	2290	4.77
		1.00	18.6	1900	4.35
		1.50	22.3	1520	4.16
		2.00	27.6	1410	4.70
	6.0	0.20	19.5	9930	15.8
		0.25	18.6	7600	11.6
		0.30	19.8	6720	10.9
		0.35	18.5	5400	8.16
		0.40	18.6	4740	7.26
		0.50	19.5	3990	6.42
		0.75	23.2	3160	6.12
		1.00	26.3	2680	5.91
		1.50	31.1	2120	5.40
		2.00	37.1	1890	5.79
130	2.1	0.20	3.32	1690	1.37
		0.25	3.39	1380	1.15
		0.30	3.64	1240	1.10
		0.35	3.97	1160	1.11
		0.40	4.00	1020	0.99
		0.50	4.80	980	1.12
		0.75	6.24	848	1.21
		1.00	7.42	757	1.23
		1.50	9.30	632	1.21
		2.00	9.75	497	0.99
	4.0	0.20	7.68	3920	3.81
		0.25	7.38	3010	2.80
		0.30	7.32	2490	2.31
		0.35	7.74	2260	2.21
		0.40	8.21	2090	2.16
		0.50	9.29	1900	2.20
		0.75	12.2	1670	2.50
		1.00	14.7	1500	2.64
		1.50	18.7	1270	2.76
		2.00	21.4	1091	2.68
$\pm$1%	$\pm$2%	$\pm$2%	$\pm$8%	$\pm$5%	$\pm$10%

Table 9: PT5 performance data for capacitance values of of 130 and 270 $\pm$2 μF and energy levels of 2.1, 4.0, and 6.0 $\pm$0.1 J. The last row in the table is the average error from each measurement.

Part II
Research by Subject

This part of the review is designed for those readers who would rather see information presented by subject in GFPPT research rather than the entire body of work from each particular laboratory alone. With that in mind, much of the information presented in this part of the review is duplicated from Part I including the relevant citations, but not figures or tables. Some additional work that is not from any of the major laboratories or was related to work in other fields and not presented in Part I are also cited in the sections on current sheet structure and acceleration model development.

7 Current Sheet Structure

Two laboratories (General Dynamics run by Lovberg, and Princeton by Jahn in the 1960's) made investigating the current sheet structure their primary task. Their research will be presented, first, individually, then used in a discussion subsection that covers all work related to current sheet canting that this author could find in the literature. Some interesting trends dealing with the permeability of the sheet and its effectiveness as a "snowplow" will be discussed in a following section on performance scaling.

7.1 Current Sheet Structure Research at GD

In the current sheet studies at General Dynamics, Lovberg used electric field and B-dot probes [7, 9] as well as Schlieren photography to investigate the nature of the current sheet and acceleration process in both parallel-plate [14] and coaxial [15] geometries using mainly hydrogen for propellant. One of the main questions he was trying to answer was if the current sheet behaved as a snowplow or a strong shock-wave.

In the parallel-plate geometry, he saw a very planar, thin current sheet that had an electron density ten times that of the ambient pre-pulse density. In addition, probe data on arrival time agreed well with the visual indications of the front. He concluded that the sheet *did* behave as a snowplow effectively sweeping up all the gas in front of it. He also found that there was a strong polarization field within the sheet and speculated that the electrons were conducting all of the current, experiencing a Lorentz force which then slightly separated them from the ions. The polarization field that develops as a result of this separation was measured to be enough to explain the subsequent ion acceleration. Using gases such as nitrogen and argon, however, he saw the sheet "bifurcate" near the anode with the bulk of the current being carried on a canted sheet, anode leading cathode. He did not study this phenomenon in depth but suggested that it was a result of the higher molecular weight, and subsequent larger gyro-radii,

of nitrogen and argon molecules. Regardless of propellant, Lovberg noticed a thin but strong density gradient in a small layer all along the cathode surface.

In the coaxial geometry using hydrogen, nitrogen, and argon, he saw very different features depending on polarity and molecular weight. In some of his earliest papers using hydrogen, Ref. [7, 9], the center electrode was at negative potential (cathode) and the current sheet seemed to be planar from field probe measurements. With the sheet speed measured from probe data being about twice that expected from a snowplow model, and the fact that the current sheet itself was *not* bowed outward due to the $1/r^2$ Lorentz force profile, he concluded that the sheet did *not* behave like a snowplow. Electric field data showed a similar polarization field to that seen in the parallel-plate geometry, however, it dropped off towards the anode. Although this might be expected with a non-uniform Lorentz profile, the polarization field was no longer strong enough for the ions to be accelerated to the observed sheet speed near the anode. Lovberg postulated that that the current sheet was permeable and acted more like a strong shock-wave in this case. In another case with reverse polarity, using the Schlieren technique (with a slotted outer electrode, Ref. [15]) the current sheet was seen to separate into two layers. The leading, thin sheet was seen to bow out along the center electrode as should be expected by the non-uniform Lorentz force in a coaxial accelerator. In the second, planar layer, he saw a much more diffuse region that did not conduct much current, possibly from a small amount of ion conduction to the cathode. Integrating the gradient information from the Schlieren photos showed that the electron density was about the same as the ambient conditions indicating that this again *did not* behave like a snowplow, rather like a strong shock. A possible explanation for this behavior was the need for ion conduction to the cathode which could leave a large number of recombined molecules near the cathode moving only with thermal speed, much slower than the sheet speed. The presence of strong radial density gradients near the cathode seemed to agree with that theory.

The coaxial thruster tested by Lovberg showed some interesting features depending on polarity. Although Schlieren photos showed a front that seemed to expand depending on the Lorentz force (bowed outward near the inner electrode) regardless of polarity, electric probe data for the cathode-center configuration showed a very planar current conduction zone. It could be possible that in the negative polarity the non-uniform Lorentz force profile is balanced by some other effect that normally causes canting with the anode leading the cathode. Other researchers have also seen effects from changing the polarity of a coaxial geometry which will be covered in more detail in following subsections.

7.2 Current Sheet Structure Research at Princeton

Three PhD thesis [46, 47, 48] and three journal publications [49, 50, 51] by Burton, Ellis, and York, respectively, examined the structure of the current sheet through electric and magnetic field probing, microwave interferometry, and fast-response pressure measurement. These three sources will be combined (Note: Ref. [50] provides the best summary of the work as it is published after

all the work had been completed) to form a coherent picture of current sheet structure as developed at Princeton. Although all of these measurements are taken at the midline of the z-pinch apparatus and at a radius half-way between the outer insulator and the center, there is no reason to think that a similar structure shouldn't exist in other pulsed accelerators with different geometries. The reader should consult all of these references for the entire story including the model development between references. Only the most simple, coherent results will be reproduced here.

First, the author's start with a generalized Ohm's Law in the frame of the moving current sheet (current sheet moves in *radial* direction in a z-pinch),

$$\vec{j} = \sigma_0 \left(\vec{E} + \vec{v}_i \times \vec{B} + \frac{\nabla P_e}{n_e e} \right) - \frac{\Omega_e}{|B|} \vec{j} \times \vec{B}. \tag{18}$$

where v_i is with respect to the current sheet velocity, and E is the net field including the applied field and the back emf contribution from the moving sheet. Note that the Hall conductivity for the electrons (but not the ions) was included because the chamber dimensions were assumed to be much larger than the electron gyro-radius, but smaller than the ion gyro-radius. Also, the effects of ion-slip (sheet permeability) were not included, and an assumption of complete, single ionization occurring as soon as the molecule enters the sheet was held throughout the publications. The electric and magnetic fields were measured with probes [49] while the scalar plasma conductivity, plasma temperature, and density were measured by microwave interferometry [50]. The Hall parameter was inferred from these measurements as was the electron pressure from the kinetic relation, $P_e = n_e k T_e$. Only the azimuthal magnetic field was found to be significant while, similarly, only the radial and axial components of the electric field were found to be important. In the frame of the current sheet, the radial ion velocity is assumed to start at sheet speed (measured from streak and Kerr-cell photos as well as probe arrival time data) and slow to zero, eventually traveling with the current sheet. As the axial current density is known from total current measurements as well as magnetic field probe data, only two unknowns remain: the radial current and the axial ion velocity. Measurements of these parameters as a function of time as the current sheet sweeps by are presented in Figure 14.

It should be noted that the axial electric field should be expected to be very nearly balanced by the back EMF of the moving current sheet so that the axial electric field actually dominates the conductivity. As seen from the measurements, this was found to be true with the appearance of three regions bounded by the character of the radial electric field. In Region I, the radial electric field is very large caused by the separation of the electrons caught on an $E_r \times B_\theta$ drift while the ions have a large momentum and penetrate deeper into the sheet with only a slight deflection towards the cathode. This radial electric field does, however, slow down the ions into Region II, although it emphis not enough to slow the ions down completely to sheet speed. Region I was found to be dominated by axial electron current making up a significant fraction of the total current, but *not* the *entire* current. Region I was found to be about

5 mm thick for argon. As the separation of the ions and electrons induces a radial polarization field, it also creates a radial current. This radial current, although relatively small, interacts with the azimuthal field enough to cause the ion trajectories to deflect even more towards the cathode. In Region II, with the ions now moving slower and slightly deflected, *axial ion current* dominates with ions recombining on the electrode surface to complete the total current. Burton suggested that this produces a $j_{iz} \times B_\theta$ that further decelerates the ions to sheet speed. Region II was also found to be the location of a large heavy species pressure gradient. As the radial electric field actually reverses sign (although not to the same magnitude) in Region II, the electrons actually try to drift against the current flow, however, with the greater ion density, collisions dominate and they remain relatively stationary with respect to the sheet. In Region III, the axial electric field is still negative, although smaller and returning to zero. As the ion density is low here, there is actually the possibility of a small reverse current being carried by the electrons in the trailing edge of the current sheet. The total sheet was found to be about 1 cm thick at the center line with a slight tilt, anode front leading cathode. At that time, no explanation was given for the tilt.

This tilt or cant of the current sheet has been investigated in more recent work at Princeton [52]. In brief, optical measurements of sheet speed and tilting angle have qualitatively found that larger molecular weight propellants experience more canting, and that the canting angle is independent of initial voltage or peak current. Research is continuing with Schlieren photography and a further discussion is presented in the next subsection.

7.3 Current Sheet Canting

From Lovberg's work and others it is clear that the molecular weight of the species plays an important role in determining the degree of canting. Using the same parallel-plate apparatus, Lovberg did not see canting with hydrogen, but did, in fact, see it using nitrogen and argon. Recent work at Princeton (Ref. [52]) has begun to study the degree of canting based on a parametric analysis of propellant species, gas density, and magnetic field (initial voltage and current) strength.

Other researchers who have observed canting include Keck at Avco-Everett who, like Lovberg, saw significant differences in magnetic probe data depending on the polarity of his coaxial accelerator using argon [58]. For the positive polarity, anode center, he noticed a 2 cm thick sheet that was tilted out along the anode. Although this result is to be expected from the stronger Lorentz force near the center electrode (regardless of polarity), he observed different behavior with reverse polarity. With the cathode as the center electrode, he noticed a very planar but thicker, 4 cm, current sheet that moved slightly *slower* than the positive polarity. In the same company, Fishman and Petschek tried to explain this phenomenon by combining the non-uniform Lorentz force and the assumption that the ions must carry a significant part of the current by recombination on the cathode [59]. In both polarity case, the non-uniform

Lorentz force and potentially a precursor shock-wave were suspected to push some of the propellant towards the outer electrode. When the anode is the center electrode the ions are pushed toward the cathode which is considered the "normal" mode and the total current can be accounted for easily. If the center electrode is the cathode, however, now the ions are forced to move *away* from the cathode. With insufficient electrode emission at the cathode, the ions must slowly diffuse to the cathode against the Lorentz force, potentially spreading out and slowing down the current sheet due to the higher plasma resistance. Fishman and Petschek's model also suggests that a relatively large amount of mass might be left behind near the outer electrode in a "bubble" where the current sheet has a smaller current density and is more permeable.

In yet another experiment, Liebing observed canting in a parallel plate accelerator using argon and a lumped transmission-line energy source [60]. Using streak cameras and magnetic field probes, Liebind found that the luminous front matched well with the current conduction zone and that the anode *always* led the cathode. He reversed polarity and found a similar result with evidence of an "anode foot" that was spread out with a lower current density than that observed at the cathode. A bright spot noticed near the cathode was suggested to be from radiation of plasma left behind the sheet. Finally, in another separate experiment using a ruby laser Schlieren system and a parallel-plate geometry, MacLelland noticed similar canting effects, although more pronounced with argon than hydrogen [61]. Still, even in the hydrogen discharges, the sheet eventually becomes canted with long enough electrodes and pulse duration. MacLelland also saw that, in a region near the cathode, the sheet was fairly planar and that an "anode foot" developed into the final canted structure.

With all of these researchers observing canting in pulsed accelerators, only two really tried to explain the reasons why it occurred in detail. In Ref. [62], Bostick examined a coaxial geometry and suggested that Hall currents combine with the normal, radial electron conduction current to give a total current deflected an angle. He also suggested that the current loops required for these near-axial Hall currents could be accounted for through the inclusion of "plasma vortices" within the current sheet that result from the sheer as the tilt develops. His evidence for such vortices was from the oscillating magnetic and axial electric field data he (as well as others he cited) had collected. In Ref. [63] Johansson, yet again at Avco-Everett, examined the current sheet tilt in an inverse z-pinch with hydrogen and argon at similar pressures. In this experiment, UV photo-detectors and magnetic field coils were used to measure the progression of the sheet. Like MacLelland, Johansson noticed an eventual canting in *both* hydrogen and argon discharges, although the tilt in hydrogen only occurred in a region near the anode. Near the cathode, the sheet was seen to be more planar with hydrogen, but the cant consumed the entire discharge in argon. At similar pressures, 100 mT (same H_2 and Ar number density), and using a separate high-voltage system to provide uniform initiation, Johansson saw that the tilt angle was similar between the two gases *as a function of radius* with the hydrogen discharge traveling almost twice as fast. In more extensive tests with argon at low pressures, he found that the trajectory of the center-of-mass

of the sheet propagated as expected from a snowplow model. At higher pressures, the luminous region ran slightly ahead of the center-of-mass indicating a slightly permeable current sheet. The tilt angle as a function of radius (tilt angle increases slightly with radius) was similar at all the pressures although the current sheet was very diffuse at the highest pressures making it difficult to quantify exactly. Johansson postulated that since the cathode could not be capable of producing the necessary electrons to conduct the total current, that ions must be the dominant current carriers near the cathode. He calculated the height (distance from the anode) where ions were assumed to carry *all* of the current as,

$$h_0 = \frac{1}{q}\sqrt{\frac{2M_w}{\mu_0 n}}, \tag{19}$$

where q is the charge of the ion, M_w is the molecular weight, and n is the ambient fill number density. He found this estimation to be roughly correct compared to his own data, Lovberg's and others.

In all of these research projects it seems that ion conduction, molecular weight (gyro-radius), number density, and the lack of sufficient electron conduction from the cathode (possibly surface effects) are involved in the canting effect. Canting has been observed in parallel-plate, coaxial, z-pinch, and inverse z-pinch geometries with the anode always leading the cathode. Although it appears that many researchers are satisfied with their own explanation, a unified theory that yields the canting angle (or how to eliminate it altogether) as a function of accelerator design parameters such as electrode separation, propellant type, total current, etc. requires further, more detailed, investigation.

8 Acceleration Model Development

Researchers in almost every program studying pulsed plasma accelerators used an acceleration model (only the more detailed studies will be covered here) that consisted of an effective circuit equation representing the discharge elements, and a momentum equation that usually included a coupling term between the motion of the discharge and the effective driving circuit. It is this driving term that makes the typically one-dimensional equation set non-linear and impossible to solve analytically without making some severe approximations to uncouple the equations. In general, there are two classes of solutions, those using a constant mass (a "slug-mass" approximation) and those including the sweeping up of mass as the current sheet progresses. The earliest work which suggested that the current sheet acts like a "snowplow" can be found in Ref. [41] where Rosenbluth examined an infinitely thin sheet with no plasma resistance.

In one of the first papers on an acceleration model for plasma thrusters, Republic Aviation used a non-dimensional slug-model for the propellant eliminating any dynamic efficiency effects [30]. They also did not include any effects of plasma resistance, wall effects or radiation, although they did include a linearly distributed resistance for the electrodes. They tested two cases depending

on integration time, however, they did not use a computer to solve the equations. The "long time" model used asymptotic analysis to integrate the circuit and momentum equations out to an effective infinite time later. As any solution to the these equations shows a damped current waveform, the current flowing through will be zero and the velocity will be constant at the end of the integration. Using this technique, the energy stored in the magnetic field and capacitor are also zero by the end of the integration. Along with the simple slug-mass assumption and without including the plasma resistance (instead, using a *constant* electrode resistance), this allows the equations to solved at t=∞. The solution given for the efficiency is,

$$\eta(t=\infty) = 1 - \frac{2}{1+\sqrt{1+EL'^2/2m_{bit}R_0^2}}, \tag{20}$$

where $L^{'}$ is the inductance-per-unit-length, E is the energy per pulse, m_bit is the slug-mass accelerated, and R_0 is the constant resistance of the electrodes. The "short time" model assumed that the sheet motion was weekly coupled to the external circuit, i.e. that the inductance was *constant*. This assumption makes the problem linear with separate, analytic solutions to the circuit and momentum equations. Again assuming a constant resistance,

$$\eta_{st} = \frac{1}{8}L'^2\frac{E}{m_{bit}}\frac{1}{R_0^2} = \frac{1}{2\sqrt{2}}\frac{L^{'}}{R_0}\bar{u}_e. \tag{21}$$

Including the effects of linear electrode resistance introduces a small correction and gives a cut-off for the initial inductance value where efficiency begins to decrease,

$$L_0 \leq \frac{R_0^2 C}{9}. \tag{22}$$

Otherwise, the initial inductance *does not* enter into the efficiency.

The non-dimensional slug model for acceleration presented in Ref. [30] is interesting in that it provides a resistance that varies as the current sheet moves down the electrodes, however, they found this to be a minimal effect. Their "short time" solutions do not include the effective resistance generated by the current sheet motion. Although this uncoupled model does not represent the electro-mechanical system correctly, it does provide a base for understanding the performance scaling. Their "long time" solution includes the effects of changing inductance, however, it does not include the effects of subsequent discharges typically found in accelerators with an oscillatory current. It also does not take into account the finite length of electrodes and corresponding maximum change in inductance for a given geometry. Still, with all of these assumptions in mind, it does produce an interesting scaling relation for a slug-like mass, Eq. 20, that with Eq. 21, shows a monotonic increase in efficiency with increases in inductance-per-unit-length and energy, and decreases in mass bit and external resistance.

In Ref. [28], Hart used a slug-mass circuit model that was solved using a computer and only at a few conditions. Although Hart recognized that the

solutions could not be realized in the experimental accelerators with ambient fills, he thought that the results might apply reasonably well to pulse-injected systems. Hart showed, as expected, that not as much energy goes into internal modes of the plasma for slug-like distributions with a corresponding increase in efficiency. Current waveforms predicted from this model were close to critically damped in character indicating a large rate of inductance change which, in reality, would require long electrodes. Hart also examined a constant mass distribution snowplow model and found very different waveforms depending on gas density. Hart also showed that a snowplow model could be modified slightly to account for the finite thickness of the current sheet although it did not significantly effect the results unless the thickness was on the same order as the thruster electrode length. In later work [29] Hart presented a modified snowplow model for coaxial accelerators with very small inner electrodes. The modified model was required to explain his experimental sheet velocity measurements, although a significant amount of unaccounted for Teflon insulator was probably the cause of the deviation from normal models.

Another slug-model developed at NASA Lewis and described in Ref. [37], actually included snowplow-like effect for mass that was eroded from the electrodes and accumulated as the current sheet progressed. As can be expected, the performance in this model strongly depended on a mass ablation coefficient that determined the ratio of ablated mass to injected propellant mass. The overall trends, however, showed a similar global result to other one-dimensional models with the highest predicted performance corresponding to large values of inductance-per-unit-length, initial voltage, capacitance and small values of initial inductance and resistance.

A more advanced, non-dimensional model developed later at Lewis and presented in Ref. [36] used a distributed propellant mass and included terms for ionization energy losses, radiation losses, wall drag due to ion diffusion, and heat transfer from the plasma to the electrodes through the inclusion of a plasma energy equation. The inclusion of the plasma energy equation included the following assumptions:

- The mass distribution function is not related to any physical phenomenon; that is, it does not have an exponential or linear nature that would be expected from pulsed gas injection or a uniform fill.
- Wall drag includes the loss in forward momentum from ions diffusing to the wall based solely on temperature and not current conduction.
- The internal energy of the plasma is based solely on temperature without including pressure effects. Energy is transferred to the plasma from the mass accumulation process and ohmic heating. Energy is lost from the plasma through heat conduction to the electrodes, electron current conduction, ion diffusion and recombination near the electrodes, ionization and radiation. It should be noted (by the author's own admission), however, that although ohmic heating, ionization, and radiation losses appear in the equations, they are not included in the actual solutions.

- The initial temperature is not specified explicitly in Ref. [36] and no profiles for plasma temperature are mentioned or displayed.

The effects of introducing the plasma energy equation are present in comparing the results of the more advanced model with one that does not include these losses, as shown in Figure 12. In general, the efficiency is found to follow a similar trend, peaking at a particular "Mass Loading Parameter" that is slightly smaller than what is predicted by the simplified model. The relative loss is smallest at small values of the Mass Loading Parameter. The Mass Loading Parameter is defined as,

$$\mathcal{M} \equiv \frac{2\ell m_0}{L' Q_0^2} = \frac{\ell m_0}{L' C E_0} \tag{23}$$

which includes the amount of mass in the initial discharge (m_0), the initial energy (E_0) or charge (Q_0) on the capacitor, the capacitance (C), the inductance-per-unit-length ($L^{'}$), and the length of the electrodes (ℓ), but *not how the mass is distributed*. This definition makes it hard to differentiate between the various parameters, and its experimental value strongly depends on the initial mass taken up by the current sheet, a very difficult quantity to determine. The authors suggest that the largest loss is through ion diffusion to the walls and that radiation losses are negligible, although they do not provide magnitudes, relative or absolute. They also suggest that radiation cooling could play a significant role, although it is not included in the final plasma energy equation. Although the model did not seem to match well with experimental data, this could have been as much a result of trusting calorimetry performance data then the fault of the model. Without more information on the temperature profile as a function of time, it is hard to say if the plasma energy equation and the associated assumptions were reasonable. Finally, it should be noted that the advanced model did not take crow-baring into account and used a non-dimensionalization scheme based on the final inductance of the current sheet at the end of the electrodes. The integration was carried out until the current sheet reached the end of the electrodes.

The simplified model that did not include the plasma energy equation did, however examine the effects of crow-baring at a beneficial time when the current is zero (no energy is stored in the magnetic fields) and at the worst time when the current is maximum. In general, the effects of choosing an appropriate crow-barring time were more pronounced than those observed from the addition of the various loss mechanisms with up a 40% performance reduction predicted using the "maximum current" crow-bar time. Experimentally, the crow-bar time was seen to depend on accelerator geometry, especially near the breech. Later geometries included an "inhibitor ring" that delayed the crow-bar to when the total current was smaller. The performance measurements are presented in more detail in the section on work at NASA Lewis in Part I, however, in general, they did not match the predictions in either absolute values or functional form. The author's explain this discrepancy based mainly on the assumed initial mass density profiles.

Researchers in Italy followed almost the same exact non-dimensional scheme as Lewis' simplified model in their acceleration model studies [64]. Their model, however, also assumed infinite conductivity of the plasma and driving circuit leaving the expanding current sheet as the only impedance. This assumption led to underdamped waveforms in almost every solution. A gaussian propellant distribution was also examined and produced a result similar to the mass-loading distribution used by Lewis. The research at Italy mainly contributed two things: 1.) As it was developed in 1972, computers were far enough along in their development to provide a large number of solutions for a wide range of parameters. 2.) A second, quasi-2D model examined the non-uniform Lorentz force in coaxial accelerators and found very different current sheet profiles depending on the *radial* propellant loading. This second model, however, did not make any correction for the canting effect noticed in many coaxial geometries and discussed previously.

At Princeton, Jahn included a comprehensive study of acceleration models in his book [1]. Pulling information from similar models in the literature, he used a non-dimensional approach based on the initial conditions for a parallel-plate accelerator. He examined the current waveforms and resulting current sheet trajectories for both slug and uniform propellant distributions. In a later non-dimensional model developed at Princeton, the effects of an expanding electrode geometry and an exponential mass distribution expected from kinetic theory were included along with the normal constant plasma resistance and snowplow models [45]. In the results from this model, tested over a wide range of parameters, the performance was seen to behave differently depending on the nature of the current waveform. In general, the efficiency increased with decreasing circuit resistance, however, for the underdamped cases with a uniform propellant fill, a maximum in the efficiency was found with a Dynamic Impedance Parameter, α, value near unity,

$$\alpha = \frac{L^{'3} V_0^2 C^2}{18 L_0^2 m^{'}}, \tag{24}$$

where $m^{'}$ is the mass density gradient coefficient. For critically or overdamped cases with a uniform fill, the efficiency increased with $\alpha^{1/4}$ yielding,

$$\eta \propto \sqrt[4]{\frac{8 L^{'3} V_0^2}{9 R_0^4 m^{'}}}, \tag{25}$$

with R_0 (including only the internal capacitor resistance and the plasma resistance) having the strongest influence. The thrust-to-power ratio *decreased* with increasing α for the underdamped cases and remained relatively constant over α for the critically or overdamped cases. Using an exponential mass distribution increased the efficiency and thrust-to-power ratio in accordance with the dynamic efficiency improving. The character of the efficiency was also changed for the underdamped case with the maximum point shifting to much higher values of α, > 10. Higher values of α, however, were also seen to require very long electrodes with total inductance changes on the order of $100 \times L_0$ which are

very difficult to achieve in reality. The nature of the thrust-to-power ratio did not change for the exponential mass distribution. Using flared electrodes also improved performance, but not to the same extent as the non-uniform propellant density. Further development of this model including crow-baring for the underdamped cases and finite-length electrode effects are ongoing at Princeton.

9 Estimates of Performance Scaling

This section differs from the previous section on acceleration models in that it specializes in how these acceleration models predict performance scaling. Many of the models mentioned earlier were not used explicitly to determine performance scaling, rather to check the trajectories of current sheets observed experimentally and determine the sweeping efficiency. Part of the reason why the early models did not search out more general trends is due to the lack of computer resources to examine a wide number of cases and develop trends. In addition, experimentally observed effects such as current sheet permeability as a function of the driving circuit and propellant loading were not included in the models. Simple estimates of performance based on both empirical data as well as simple acceleration models have paved the way for improvements in GFPPTs.

The first simple scaling relation came from the asymptotic solutions of a slug-model studied at Republic Aviation [30]. In that model, the efficiency was seen to scale as:

$$\eta(t=\infty) = 1 - \frac{2}{1+\sqrt{1+EL'^2/2m_{bit}R_0^2}}, \tag{26}$$

where $L^{'}$ is the inductance-per-unit-length, E is the energy per pulse, m_bit is the slug-mass accelerated, and R_0 is the constant resistance of the electrodes. In another "short time" model, it assumed that the sheet motion was weekly coupled to the external circuit, i.e. that the inductance was *constant*. This assumption makes the problem linear with separate, analytic solutions to the circuit and momentum equations. Again assuming a constant resistance,

$$\eta_{st} = \frac{1}{8}L'^2\frac{E}{m_{bit}}\frac{1}{R_0^2} = \frac{1}{2\sqrt{2}}\frac{L^{'}}{R_0}\bar{u}_e. \tag{27}$$

Including the effects of linear electrode resistance introduces a small correction and gives a cut-off for the initial inductance value where efficiency begins to decrease,

$$L_0 \leq \frac{R_0^2 C}{9}. \tag{28}$$

Otherwise, the initial inductance *does not* enter into their efficiency estimates. These results show a monotonic increase in efficiency with increases in inductance-per-unit-length and energy, and decreases in mass bit and external resistance.

In more recent work at Princeton, a similar, fixed element approximation [44] for performance scaling has been developed for coaxial and parallel-plate electrode geometries. In the fixed element solution, primarily modeling a critically

damped waveform, the inductance was assumed not to change (although it was given an *average* value, $< L >$, greater than the initial inductance, L_0), and the effective resistance was also held constant. The impulse was assumed to depend solely of the integral of the current squared with the final relation showing a linear dependence on the initial energy stored in the capacitor,

$$I_{bit} = L^{'}\sqrt{\frac{C}{< L >}}E. \tag{29}$$

The efficiency was predicted as,

$$\eta = \frac{I_{bit}^2}{2m_{bit}E} = \frac{1}{2}L^{'2}\frac{C}{< L >}\frac{E}{m_{bit}} = \frac{1}{2}L^{'}\sqrt{\frac{C}{< L >}}\bar{u}_e. \tag{30}$$

Note that in this approximation, the average inductance quantity depends on the position of the current sheet and the inductance-per-unit-length. In this way, the efficiency could also be considered to depend on $\sqrt{L^{'}}/\sqrt{\ell_{elect}}$. In any case, both the impulse bit (thrust-to-power ratio) and the efficiency are expected to scale with a square-root of capacitance. A similar relation can be found in Ref. [65].

In a more complicated snowplow model for a z-pinch at Princeton [40], the model results were put together with experimental data to find that, when the sweeping efficiency was high, the sheet velocity was seen to scale with the non-dimensional "magnetic interaction parameter" β,

$$\beta \equiv -\frac{\mu_0 Q_0^2}{4\pi^2\rho_0 r_0^4} = -\frac{\mu_0}{2\pi}\frac{h}{r_0^2}\frac{CE}{m_{bit}}, \tag{31}$$

where ρ_0 is the initial density, r_0 is the outer electrode radius, and h is the distance between the electrodes. Various values of the β parameter were investigated using different mass densities and outer electrode radii. The pinching effect was also found to be a strong function of β with the pinch occurring *before* the current reversal for $|\beta| > 0.2$.

In another, non-dimensional model including the effects of a flared electrode geometry and an exponential mass distribution [45], the performance was seen to behave differently depending on the nature of the current waveform. In general, the efficiency increased with decreasing circuit resistance, however, for the underdamped cases with a uniform propellant fill, a maximum in the efficiency was found with a Dynamic Impedance Parameter, α, value near unity,

$$\alpha = \frac{L^{'3}V_0^2C^2}{18L_0^2m^{'}}, \tag{32}$$

where $m^{'}$ is the mass density gradient coefficient. For critically or overdamped cases with a uniform fill, the efficiency increased with $\alpha^{1/4}$ yielding,

$$\eta \propto \sqrt[4]{\frac{8L^{'3}V_0^2}{9R_0^4m^{'}}}, \tag{33}$$

with R_0 (including only the internal capacitor resistance and the plasma resistance) having the strongest influence.

In the non-dimensional model developed at NASA Lewis [36] and used again at the University of Pisa [64], the optimal performance over many operational parameters occurred when the Mass Loading Parameter was near unity. The Mass Loading Parameter is defined as,

$$\mathcal{M} \equiv \frac{2\ell m_0}{L' Q_0^2} = \frac{\ell m_0}{L' C E_0} \tag{34}$$

which includes the amount of mass in the initial discharge (m_0), the initial energy (E_0) or charge (Q_0) on the capacitor, the capacitance (C), the inductance-per-unit-length ($L^{'}$), and the length of the electrodes (ℓ), but *not how the mass is distributed*. This definition makes it hard to differentiate between the various parameters, and its experimental value strongly depends on the initial mass taken up by the current sheet, a very difficult quantity to determine.

In experimental performance scaling experiments, it is interesting to note that thrusters with current rise rates per unit width of less than $10^{12} A/(m \cdot s)$ have empirically been shown to have less than 100% sweeping efficiency [1, 40]. In the case of Lovberg's experiments where he found mixed results [7, 14], this criteria holds true: the parallel-plate accelerator has a width of 8 cm and a current rise rate of 250e9 A/s giving about 3e12 A/ms while the coaxial geometry has an average width of 22.6 cm and a current rise rate of 160e9 A/s giving about 0.7e12 A/ms. In accordance with the rule of thumb, the parallel-plate thruster showed behavior like a snowplow while the coaxial geometry did not. In another coaxial geometry tested later at GD [11], a higher capacitance and smaller average radius electrodes reached up to 1.4e12 A/ms [11]. Although the authors did not expressly try to match or exceed this criteria at the time, probe data confirmed that the current sheet was indeed acting like a snowplow in this later, coaxial device. This rule of thumb applies well to almost any geometry as demonstrated in other experiments as well, frequently without the authors realizing that they did meet the criteria [19, 35, 63]. It is also interesting to note that in many experiments where the sheet was classified *not* to be an effective sweeper [7, 28, 39], the sheet velocity scaled as the *square-root* of the energy to mass ratio as apposed to an expected linear scaling as predicted for effectively sweeping sheets [14, 31, 40, 63]. In Ref. [54], Guman showed with a relatively simple model that the square-root scaling would be expected for an electrothermal acceleration mechanism. The linear relation is expected for electromagnetic acceleration as shown in Eq. 30.

Many experimental performance scaling studies have been completed in GF-PPT research, although, unfortunately, many of them have not been controlled experiments. That is to say that instead of varying only one parameter (capacitance, for example) at a time, most researchers enact many changes at once, sometimes without even realizing it. Therefore, any conclusions they make about their modifications cannot be attributed to a specific change in one parameter and the specific scaling relation is unclear.

At General Electric, following many, multi-parameter modifications [20], the efficiency was shown to be linear with exhaust velocity over a wide range of mass bits (smaller mass bits gave higher efficiency) with a relatively constant thrust-to-power ratio near 20 μN/W at similar capacitance and discharge energy levels [21]. GE also conducted a performance survey over five different capacitance values from 50 to 200 μF to find that the performance scaled with the square-root of the capacitance to within 5-10% [23]. As discussed in the sections on research at GE and GD in Part I, however, GE's performance measurements have the possibility of including facility background-contamination. This may add doubt to their *absolute* performance measurements, but perhaps their *scaling* trends are more acceptable.

Hart may have been the first one to realize that a solid-propellant Teflon thruster could have space-flight applications (see footnote in Ref. [29]. Although he tested a variety of geometries, capacitance, inductance, and mass bit values, unfortunately all of his experiments were influenced by the ablation of a significant amount of Teflon from the backplate. With gas propellant mass bits between 10 and 500 μg and discharge energy levels being a 1 kJ or higher, The majority of the discharge could easily have been made up of Teflon at the lowest, middle, and even highest mass bits for the small inner electrodes. Although his computation models are valid (except possibly the modified form of the snowplow model), the results from streak photos that do not distinguish the radial position of the current sheet do not provide an adequate comparison or verification of the models. The "Mode II" operation showing the fastest sheet speed is probably a result of a canted current sheet leading down the center electrode (anode) much faster than the true plasma center-of-mass.

At Princeton, the performance of a low-energy, high-rep-rate GFPPT was studied parametrically. Two energy levels for each of two capacitance values were tested over ten different mass bit values each yielding a 40-point GFPPT performance database. Four graphs which show PT5 performance as a function of mass bit and specific impulse with the capacitance and the initial stored energy level as parameters are shown with error bars in Fig. 18. Each point represents at least twenty trials including separate measurements of impulse, mass bit, and energy at the same conditions. Values of the performance data are given at the end of this section in Table 9. It is evident from all the plots in Fig. 18 that for each curve there is a transition with decreasing mass bit (or increasing I_{sp}) from a mode (Mode I) where the efficiency and the impulse are respectively independent and dependent on the mass bit (and where the efficiency the thrust to power ratio are respectively independent and dependent on I_{sp}) to another mode (Mode II) where the converse statements hold.

Simple analytic models presented in the previous section show that the efficiency and thrust-to-power ratio should scale with the square-root of capacitance and not depend on the energy (at a constant exhaust velocity) for an electromagnetic accelerator. These trends are evident in Mode II where the efficiency increases linearly with the specific impulse and the thrust-to-power ratio is relatively constant.

It is interesting to note that the performance scaling suggested for a thruster

where electrothermal acceleration is dominant are quite different (again, see Ref. [54]). In that case, the impulse bit is expected to scale with the square root of the discharge energy to mass bit ratio and not depend directly on capacitance or inductance change. In addition, the efficiency of a pure electrothermal accelerator is expected to be constant over wide range of specific impulse, energy and mass bit values. While the efficiency as seen in panels c and d of Fig. 18 is indeed independent of mass bit and I_{sp} at high mass bit values (i.e. Mode I), it does show a dependence on energy, albeit a weaker one than for Mode II. This tends to indicate that the acceleration in Mode I may be due to a combination of both electrothermal and electromagnetic effects. Again, as the losses associated with sweeping up the propellant are not accounted for in these predictions, an explanation for trends in Mode I could be a function of improved dynamic efficiency as well.

In general, all the models and experimental evidence points to using high-voltage, high-capacitance, high-inductance-per-unit-length, low mass discharges with a minimum of parasitic inductance or resistance and short electrodes. Current sheet permeability, propellant utilization efficiency, and the potential problems of crow-bar discharges are important to consider when designing the driving circuit as well. Discharge symmetry, and the resulting decrease in performance from asymmetric discharges, are a result of proper discharge initiation.

10 Experimental Performance Measurements

Again, many of the experimental performance measurements have been presented before, however they will be repeated here to some extent. The measurements are divided according to research laboratory and the results are sometimes shown graphically or with tables in Part I. More details on specific geometries or the progression of GFPPT design at each laboratory can be found in Part I.

10.1 Summary of GD Performance Measurements

The measurements presented here were performed during the later stages of GFPPT development at General Dynamics [17] using a thrust stand (pulsed operation at 10 Hz gave effective "steady" measurement and average impulse bit) and an appropriately conditioned thruster to eliminate contamination effects. The capacitance was increased to a final value of 140 μF with a distributed inductance giving nearly a square current pulse. The geometry of this thruster was slightly different than that of Figure 1. The length of the center electrode was shorter (5.5 cm) with the same radius (1.9 cm) while the outer electrode was about the same length (15.8 cm) but had a larger radius (6.25 cm). The new radius ratio was about 3.3. The propellant was injected radially at the breech with the discharge initiation timing controlled by a gas-discharge switch. Propellant utilization was measured to be just over 60% with nitrogen and a 350 μs delay. The mass bit was controlled by changing the feed pressure and the quantity was determined by integrating measured density profiles. Both

nitrogen and xenon data were used in this study as shown in Tables 1 and 2 and Figures 3 and 4. In general, the efficiency varied from 6 to 56%, the specific impulse varied from 350 to 13,000 s, and the thrust-to-power ratio varied from 33.5 to 8.7 μN/W, respectively, depending mass bit and energy. As expected, the highest efficiencies corresponded to the highest energy and lowest mass bit values, however, the thrust-to-power ratio is highest at the *lowest* energy and highest mass bit values.

Thrust stand data was also obtained using a GFPPT very similar in design to General Electric's A-7D GFPPT with axial propellant flow (xenon) and a separate high-voltage discharge initiation system. GE's mass injection scheme was duplicated very closely to insure the same propellant utilization ($> 90\%$) and density profiles. While faraday cup measurements of ion velocity and exhaust beam divergence were very similar to those obtained at GE (see next section), thrust stand and performance measurement data disagreed with significantly lower values measured at General Dynamics [17]. Table 3 shows performance values at four energy levels. For this device, the efficiency is relatively constant at a fixed energy while the thrust-to-power ratio still shows a tendency to decrease with increasing energy and decreasing mass bit.

10.2 Summary of GE Performance Measurements

The measurements provided in Table 6 and Figures 6 and 7 represent thrust-stand measurements from GE's A-7D model using xenon propellant and a 144.5 μF capacitor bank with a Q-factor of 14. Unfortunately, only energy (with Q-factor reduction), specific impulse, and efficiency were given in Ref. [23] where all of this data is reported in graphic form. This is, however, the best source for pure data as GE did not frequently show many points in a data set or any tabular information. The mass bit and impulse bit values must, therefore, be inferred from the reported specific impulse, voltage, and efficiency measurements,

$$I^*_{bit} = \frac{2\eta}{I_{sp} g_0} \frac{1}{2} C V_0^2 \left(1 - \frac{1}{Q}\right), \tag{35}$$

$$m^*_{bit} = \frac{I^*_{bit}}{I_{sp} g_0}, \tag{36}$$

where the star superscript indicates the inferred quantities. Finally, it must be noted that out of every lab conducting GFPPT performance measurements on thrust stands [4, 5, 17], GE is the *only* one that did not report any decrease in measured thrust or impulse over the first 100-1000 pulses, including tests at similar mass bits and energies. As GE's protocol for measuring thrust is not published explicitly, it is unclear if any preconditioning of the thruster took place before the measurement.

Unfortunately, the researchers at GE did not mention any impulse decay effects that have been observed at three other laboratories testing the performance of GFPPTs on thrust-stands in diffusion pumped chambers [4, 5, 17]. Although researchers at GE did not notice any performance changes from changing the

pulse frequency, details of the this experiment were not given. Rather than pulse *rate*, the total number of pulses has been shown to be more important in conditioning the thruster for proper operation. Without such conditioning, adsorbed gases from the electrode surfaces and organic-monolayers from the roughing and diffusion pumps can significantly alter *both* the amount of mass in the discharge and the electrical conduction of the plasma near the electrode surface. Although these effects could be beneficial, true performance as would be expected in space operation can only be measured after a conditioning period and as long as pump oil is not allowed to migrate to the thruster electrodes.

Three other pieces of evidence suggest that the performance measured at GE might include contamination effects:

1. GE's vacuum chamber used three 32" diffusion pumps that did not have baffles of any kind to prevent back-streaming. The closest pump was less than one meter away from the thrust stand [19].

2. Gridded ion velocity measurements taken by researchers at GE showed a significant amount of carbon and oxygen ions that varied from pulse-to-pulse. Although the total mass of these atoms may not have been significant compared to the xenon ions, their source and their effect on the current sheet structure remains unknown [27].

3. General Dynamics constructed a very similar thruster to that of GE's A-7D and found, at best, a factor of two *smaller* performance [17].

The last item can best be visualized graphically with the results from Tables 3 and 6 being plotted in Figure 8. From this graph, it is easy to see that the data measured at General Dynamics has significantly lower performance than that measured at General Electric. It should be noted that General Dynamics and General Electric were competitors, however, only General Dynamics took the effects of background contaminants into account [17]. After 1970, there are no more publications from GE on GFPPTs, however, research at GE began on ablative pulsed plasma thrusters in the late 1960's.

10.3 Summary of Republic Performance Measurements

Unfortunately, the experimental work with the z-pinch, coaxial hybrid thruster never produced an efficiency calculation in the journal publications. They were suggested to be below 50% from calculations of the amount of energy going into the internal losses of the capacitors [32]. Velocity measurements from probes do not necessarily correspond to the mass averaged exhaust velocity as the sweeping efficiency of the sheet may not be 100%. For this thruster geometry, probably the most difficult thing to calculate was the mass bit which could explain the lack of efficiency data. In the summary produced by NASA Lewis [2], efficiencies were shown to be around 14% at 3,000 s (9.5 μN/W) with nitrogen although the exact configuration of the thruster is unclear compared to the journal publications. In his last paper, Guman did measure the thrust-to-power

ratio (without specific impulse) and found that it asymptotes to about 9 μN/W at small mass loadings (previously tested conditions) and reached almost an order of magnitude higher, 80 μN/W at higher mass distributions. This was, by far, the largest thrust-to-power ratio measured for any GFPPT at the time, although the efficiency and specific impulse at this condition were probably very low. Still, the lack of continuing research on them at Republic after this measurement is puzzling, although Guman did begin ablative pulsed plasma thruster research soon afterwards.

10.4 Summary of NASA Lewis Performance Measurements

Researchers at NASA Lewis measured the performance (calorimetry) of four different accelerator designs, as shown in Table 8 and taken from Ref. [36]. The thruster was conditioned by firing ten times prior to any measurement. All the designs used mainly argon for propellant and an ignitron switch for discharge initiation timing. The propellant utilization for these devices was estimated to be 100% due to the short valve times (0.1 ms) and long barrels. The accelerators were all backed by a 12.1 μF capacitor bank that could be charged up to as much as 30 kV. Reduction in parasitic inductance came from improving the connection between the capacitor bank and accelerator as well as modifications to the gun geometry itself. Even with changes in propellant injection location, initial inductance, and inductance-per-unit-length, no noticeable difference in performance was measured until the electrode length was reduced by slightly more than 50%. Unfortunately, the inductance-per-unit-length was also changed in this configuration making the correlation with the stronger Lorentz force or reduced wall losses difficult to differentiate.

Probably the two biggest contributions from NASA Lewis are the most inclusive acceleration model published from any of the labs [36] and the review of GFPPT research in 1965 [2]. Performance measurements at Lewis did not include thrust-stand data, although the thruster was pre-conditioned to eliminate electrode contamination. In addition, although changes were made in thruster geometry, propellant distribution, and energy, they were not systematically tested so correlation between the modifications and performance improvements could only be speculated. Finally, with only a few mass bit values tested and no amount of error reported, the trends presented in the data are difficult to distinguish.

10.5 Summary of Princeton Performance Measurements

To date, nine generations of SRL-EPPDyL GFPPTs have been tested with many modifications on each generation. Using a low-voltage (250 V), low-inductance ($<$ 5 nH) capacitor bank (45-270 μF, 1.4-8.4 J), these GFPPTs have close to critically-damped current waveforms with no noticeable crow-baring. Peak currents are close to 10 kA with pulses lasting about 5 μs. As shown schematically in Figure 15, during a burst the valve is only cycled once, therefore, the ultra-fast, high energy valves used in previous GFPPT designs are not required. As

the propellant flows at a constant rate, the propellant utilization is dictated by the pulse frequency and the thermal velocity of the propellant. For example, using argon ($v_{th} \approx 400$ m/s) and a 4 kHz pulse frequency, the electrodes are required to be at least 10 cm long to ensure that none of the propellant escapes outside of the discharge volume between pulses.

Although many different GFPPT designs have been tested at EPPDyL, the fifth-generation (designated as PT5) has undergone the most extensive performance measurements. Since its original design, changes have been made to its discharge initiation system and propellant distribution [10] as well as the performance measurement technique to insure proper conditioning [5]. As shown in Fig. 16, PT5 uses a stainless-steel, coaxial electrode set with an outer to inner electrode radius ratio of approximately four and a total volume of 350 cm^3. It uses four semi-conductor type surface-flashover spark plugs mounted on the inside of the outer electrode (cathode) at 90 degree azimuthal intervals to initiate the discharge uniformly. The main discharge is driven by a low-inductance (10 nH) 130 or 270 μF capacitor bank which is capable of being charged to 250 V giving a maximum energy per pulse of 4 or 8 J, respectively. The entire thruster has a mass of approximately 6 or 8 kg depending on the capacitance level and including the electrode mass as well as the thruster housing mass. High-speed photographs of the discharge were taken with an Imacon Fast-Framing Camera (IFFT) at rates of 500,000 frames per second. A series of IFFT frames of PT5 showing the symmetrical discharge initiation are presented in Fig. 17. Before the modifications to the gas manifold were made to make propellant injection more uniform, the discharge initiation was seen to occur near the region of highest pressure. This is a similar result to those researchers who found spoking instabilities when the discharge was allowed to initiate based solely on a Paschen breakdown without an external switch.

Two energy levels for each of two capacitance values were tested over ten different mass bit values each yielding a 40-point GFPPT performance database. Four graphs which show PT5 performance as a function of mass bit and specific impulse with the capacitance and the initial stored energy level as parameters are shown with error bars in Fig. 18. Tables of the performance data are given at the end of this section. It is evident from all the plots in Fig. 18 that for each curve there is a transition with decreasing mass bit (or increasing I_{sp}) from a mode (Mode I) where the efficiency and the impulse are respectively independent and dependent on the mass bit (and where the efficiency the thrust to power ratio are respectively independent and dependent on I_{sp}) to another mode (Mode II) where the converse statements hold. More performance measurements with changing inductance-per-unit-length are ongoing at Princeton.

Part III
Summary

11 Progression of GFPPT Designs

Gas-Fed Pulsed Plasma Thrusters have been developed in many laboratories over many years. Originally developing from the magnetic shock tubes [66, 67] and applications to fusion research [6], the first plasma guns of many laboratories (see Refs. [8, 19, 28, 35] had long, coaxial electrodes with small radius ratios and propellant injection near the middle of the electrode volume. Typically these first GFPPTs were also operated at high energy (> 1 kJ) and low capacitance ($\approx 10\mu$F) with the Paschen break-down controlling the discharge initiation. Many of the designs had relatively large amounts of parasitic inductance (≈ 100 nH) and lightly damped oscillatory current waveforms where the dynamics of the discharge were dominated by subsequent crow-baring. As the designs progressed, radius ratios were more than doubled, the electrodes were shortened by almost a factor of four, the driving capacitance was increased by an order of magnitude the parasitic inductance and resistance were reduced as much as possible, and average energy was reduced to below 100 J. Some of these later devices did not exhibit crowbarring with near critically damped current waveforms while others timed the crowbar (current reversal) to coincide with the discharge reaching the end of the electrodes so that no energy stored in magnetic fields was wasted. High speed, high voltage valves were introduced from improved propellant utilization, close to 100% in many designs. The discharge initiation process was also controlled with either a high current, low inductance gas discharge switch or high-voltage spark triggers. Efficiencies of these devices were greater than 20 % at specific impulse values near 4000 s with thrust-to-power ratios close to 10 μN/W.

The progress was best summed up in 1965 where researchers at Lewis outside of the experimental group produced a comprehensive review of GFPPT research [2]. It gave the following list of important lessons learned to date:

1. Calorimetry data from many labs did not agree with the subsequent performance data measured on thrust-stands. Thrust-stand data was generally accepted as the most accurate way to measure performance.

2. Crow-baring generally occurs in all unsteady devices sometime between the voltage and current reversal points depending on thruster geometry and driving circuit parameters.

3. The main acceleration mechanism inside the current sheet was believed to be primarily due to the polarization field created by the electrons trapped on an $E \times B$ drift and the subsequent charge separation. The report also mentioned, however, that many of the labs had very different results and disagreed in this area, especially on the influence and existence of ion conduction.

4. The coaxial geometry (compared to pinch or parallel-plate) was suggested to be the best because it trapped all of the electromagnetic fields although it has a large electrode surface area and small inductance-per-unit length which decreased efficiency.

5. Including an electric switch in the discharge initiation process (as apposed to using the Paschen break-down point alone) led to better repeatability, fewer spoking instabilities, and improved propellant utilization while, at the same time, it introduced parasitic inductance and resistance as well as adding reliability questions.

6. Stated the need for a simple performance model that was confirmed by repetitive experimental performance measurements.

7. Stated that the only thing keeping GFPPTs from being used in space was their lack of "heat handling capability" and that research was shifting to quasi-steady devices which might have better performance.

Unfortunately, GFPPT research began to fade soon after this report. The two main problems were the lifetime and performance issues associated with the ultra-fast, high energy solenoid valves as well as relatively low performance and large system mass compared to other electric propulsion systems being developed at the same time (ion thrusters for example) for main propulsion. Research at General Dynamics, NASA Lewis, and Princeton shifted to quasi-steady gas fed devices where discharge times were increased and the current sheet was allowed to stabilize near the end of the electrodes. These devices did not require the fast valves of the past and showed promisingly better overall performance with the ability to process many mega-watts of power in relatively small device. At the same time, as these devices are pulsed, they share the advantage of arbitrarily lower steady-state power consumption. Still, system mass was large and this type of device did not experience in-space testing until recently with the flight of the Japanese Space-Flier Unit. Research at General Electric and Republic aviation shifted to ablative pulsed plasma thrusters that used much lower energy and were geared more towards attitude control applications. Some of these US developed devices flew in space as early as the 1970's on a Navy satellite.

Recently at Princeton, GFPPTs have resurfaced as a higher efficiency alternative to APPTs for attitude control applications, low-power deep space missions, and missions where a unique propellant requirement or contamination issues are important. These GFPPTs operate at much lower energies than their predecessors and have similar, although slightly lower, performance. The fast acting valves have been replaced by using modern, solid-state pulse-forming technology that allows > 4 kHz pulse rates and steady mass flow during the burst of pulses. The performance scaling of the devices has been measured over a wide range of operational parameters, and two modes of operation depending on propellant distribution, have been observed. The first mode has a high thrust-to-power ratio and relatively low efficiency while the second mode has

a relatively high efficiency and low thrust-to-power ratio. These thrusters are now under consideration for various space missions.

12 Future of GFPPT Research

The future of GFPPT research still lies in the general category of improving performance. Although the modern, low energy devices have achieved similar performance to the older, higher-energy devices while requiring much less massive systems, there are still areas where performance can be improved:

1. Understanding the permeability and canting of the current sheet as a function of various operational parameters and, possibly controlling them.
2. Creating a more uniform, reliable discharge initiation system that reduces erosion rates.
3. Developing ways of further reducing parasitic inductance and resistance or improving plasma conductivity especially at low energy.
4. Using higher inductance-per-unit-length electrode geometries, possibly with externally applied fields.
5. Testing the devices in space examining potential contamination, performance, waste-heat processing, and EMI effects.

References

[1] R.G. Jahn. *Physics of Electric Propulsion*. McGraw-Hill, 1969.

[2] S. Domitz, H.G. Kosmahl, P. Ramins, and N.J. Stevens. Survey of electromagnetic accelerators. Technical Report TN D-3332, NASA, 1965.

[3] O.K. Mawardi, editor. *Proceedings of an International Symposium on Plasma Guns, Pysics of Fluids Supplement (Part II, Vol. 7(11))*, November 1964.

[4] W.J. Guman and W. Truglio. Surface effects in a pulsed plasma accelerator. *AIAA Journal*, 2(7):1342–1343, July 1964.

[5] J.K. Ziemer, E.Y. Choueiri, and D. Birx. Is the gas-fed PPT an electromagnetic accelerator? an investigation using measured performance. In 35^{th} *Joint Propulsion Conference*, Los Angeles, California, June 20-24 1999. AIAA 99-2289.

[6] J. Marshal. Performance of a hydromagnetic plasma gun. *The Physics of Fluids*, 3(1):134–135, January-February 1960.

[7] L.C. Burkhardt and R.H. Lovberg. Current sheet in a coaxial plasma gun. *The Physics of Fluids*, 5(3):341–347, March 1962.

[8] T.J. Gooding, B.R. Hayworth, and R.H. Lovberg. Instabilities in a coaxial plasma gun. *AIAA Journal*, 1(6):1289–1292, June 1963.

[9] R.H. Lovberg. Inference of plasma parameters from measurement of E and B fields in a coaxial accelerator. In *Proceedings of an International Symposium on Plasma Guns, Pysics of Fluids Supplement (Part II, Vol. 7(11))*, pages S57–S61, November 1964.

[10] J.K. Ziemer, T.E. Markusic, E.Y. Choueiri, and D. Birx. Effects of ignition on discharge symmetry in gas-fed pulsed plasma thrusters. In 34^{th} *Joint Propulsion Conference*, Cleveland, Ohio, July 13-15 1998. AIAA 98-3803.

[11] A.V. Larson, T.J. Gooding, B.R. Hayworth, and D.E.T.F. Ashby. An energy inventory in a coaxial plasma accelerator driven by a pulse line energy source. *AIAA Journal*, 3(5):977–979, May 1965.

[12] D.E.T.F. Ashby, T.J. Gooding, B.R. Hayworth, and A.V. Larson. Exhaust measurements on the plasma from a pulsed coaxial gun. *AIAA Journal*, 3(6):1140–1142, June 1965.

[13] D.E.T.F. Ashby. Energy loss in pulsed coaxial plasma guns. *AIAA Journal*, 3(6):1045–1047, June 1965.

[14] R.H. Lovberg. The measurement of plasma density in a rail accelerator by means of schlieren photography. *IEEE Transactions on Nuclear Science*, pages 187–198, January 1964.

[15] R.H. Lovberg. Schlieren photography of a coaxial acclerator discharge. *The Physics of Fluids*, 8(1):177–185, January 1965.

[16] R.H. Lovberg. Investigation of current-sheet microstructure. *AIAA Journal*, 4(7):1215–1222, July 1966.

[17] A.V. Larson, L. Liebing, and R. Dethlefsen. Experimental and evaluation studies of a coaxial plasma gun accelerator. Technical Report CR-54710, NASA, 1966.

[18] D.E.T.F. Ashby, L. Liebing, A.V. Larson, and T.J. Gooding. Quasi-steady-state pulsed plasma thrusters. *AIAA Journal*, 4(5):831–835, May 1966.

[19] P. Gloersen, B. Gorowitz, and J.H. Rowe. Some characteristics of a two-stage repetitively fired coaxial gun. *IEEE Transactions on Nuclear Science*, pages 249–265, January 1964.

[20] P. Gloersen, B. Gorowitz, and J.T. Kenney. Energy efficiency trends in a coaxial gun plasma engine system. *AIAA Journal*, 4(3):436–441, March 1966.

[21] B. Gorowitz, T.W. Karras, and P. Gloersen. Performance of an electrically triggered repetitively pulsed coaxial plasma engine. *AIAA Journal*, 4(6):1027–1031, June 1966.

[22] T.W. Karras, B. Gorowitz, and P. Gloersen. Neutral mass density measurements in a repetitively pulsed coaxial plasma accelerator. *AIAA Journal*, 4(8):1366–1370, August 1966.

[23] B. Gorowitz, P. Gloersen, and T.W. Karras. Steady state operation of a two-stage pulsed coaxial plasma engine. In 5^{th} *Electric Propulsion Conference*, San Diego, California, March 7-9 1966. AIAA 66-240.

[24] B. Gorowitz, P. Gloersen, and T.W. Karras. A 20 kW solor powered pulsed plasma engine system concept. In 3^{rd} *Aerospace Sciences Meeting*, New York, New York, January 24-26 1966. AIAA 66-114.

[25] P. Gloersen. Current status of pulsed plasma engine development. In 2^{nd} *Joint Propulsion Conference*, Colorado Springs, Colorado, June 13-17 1966. AIAA 66-566.

[26] T.W. Karras and P. Gloersen. Consequences of the functional dependence of performance on various factors in a systems weight analysis of a pulsed plasma transfer. In 8^{th} *Aerospace Sciences Meeting*, New York, New York, January 19-21 1970. AIAA 70-168.

[27] T.W. Karras, B. Gorowitz, and P. Gloersen. Experimentally measured velocity distribution in the plasma stream of a pulsed coaxial accellerator. *AIAA Journal*, 4(8):1366–1370, August 1966.

[28] P.J. Hart. Plasma acceleration with coaxial electrodes. *The Physics of Fluids*, 5(1):38–47, January 1962.

[29] P.J. Hart. Modified snowplow model for coaxial plasma acclerators. *Journal of Applied Physics*, 35(12):3425–3431, December 1964.

[30] P.M. Mostov, J.L. Neuringer, and D.S. Rigney. Electromagnetic acceleration of a plasma slug. *The Physics of Fluids*, 4(9):1097–1104, September 1961.

[31] L. Aronowitz and D.P. Duclos. Characteristics of the pinch discharge in a pulsed plasma accelerator. In E. Stuhlinger, editor, *Electric Propulsion Development*, volume 9 of *Progress in Astronautics and Rocketry*. Academic Press, 1963.

[32] D.P. Duclos, L. Aronowitz, F.P. Fessenden, and P.B. Carstensen. Diagnostic studies of a pinch plasma accelerator. *AIAA Journal*, 1(11):2505–2513, November 1963.

[33] L. Aronowitz. Delays in initiation of discharges in pulsed plasma accelerators. *AIAA Journal*, 2(11):2019–2020, November 1964.

[34] W.J. Guman. Switch-triggered pulsed plasma accelerator thrust measurements. *AIAA Journal*, 3(6):1158–1159, June 1965.

[35] C.J. Michels and P. Ramins. Performance of coaxial plasma gun with various propellants. In *Proceedings of an International Symposium on Plasma Guns, Pysics of Fluids Supplement (Part II, Vol. 7(11))*, pages S71–S74, November 1964.

[36] C.J. Michels, J.E. Heighway, and A.E. Johansen. Analytical and experimental performance of capacitor powered coaxial plasma guns. *AIAA Journal*, 4(5):823–830, May 1966.

[37] D.J. Vargo. Electromagnetic acceleration of a variable-mass plasma. Technical Report TN D-2164, NASA, 1964.

[38] C.J. Michels. Some transient electrical characteristics of the exhaust of a self-crowbarred coaxial plasma gun. Technical Report TN D-2571, NASA, 1964.

[39] R.G. Jahn and W. von Jaskowsky. Structure of a large-radius pinch discharge. *AIAA Journal*, 1(8):1809–1814, August 1963.

[40] R.G. Jahn and W. von Jaskowsky. Current distributions in large-radius pinch discharges. *AIAA Journal*, 2(10):1749–1753, October 1964.

[41] M. Rosenbluth. Infinite conductivity theory of the pinch. Technical Report LA-1850, Los Alamos, 1954.

[42] N.A. Black and R.G. Jahn. Dynamic efficiency of pulsed plasma accelerators. *AIAA Journal*, 3(6):1209–1210, June 1965.

[43] R.G. Jahn, W. von Jaskowsky, and R.L. Burton. Ejection of a pinched plasma from an axial orifice. *AIAA Journal*, 3(10):1862–1866, October 1965.

[44] J.K. Ziemer, E.Y. Choueiri, and D. Birx. Trends in performance improvements of a gas-fed pulsed plasma thruster. In 25^{th} *International Electric Propulsion Conference*, Cleveland, Ohio, August 24-28 1997. IEPC 97-040.

[45] J.K. Ziemer and E.Y. Choueiri. Dimensionless performance model for gas-fed pulsed plasma thrusters. In 34^{th} *Joint Propulsion Conference*, Cleveland, Ohio, July 13-15 1998. AIAA 98-3661.

[46] R.L. Burton. *Plasma Accleration in a Propagating Current Sheet*. PhD thesis, Princeton University, 1966.

[47] W.R. Ellis. *An Investigation of Current Sheet Structure in a Cylindrical Z-pinch*. PhD thesis, Princeton University, 1967.

[48] T.M. York. *Pressure Distribution in the Current Sheet Structure of a Dynamic Pinch Discharge*. PhD thesis, Princeton University, 1968.

[49] R.L. Burton and R.G. Jahn. Acceleration of a plasma by a propagating current sheet. *The Physics of Fluids*, 11(6):1231–1237, June 1968.

[50] W.R. Ellis and R.G. Jahn. Ion density and current distributions in a propagating current sheet, determined by microwave reflection technique. *Journal of Plasma Physics*, 3(2):189–213, February 1969.

[51] T.M. York and R.G. Jahn. Pressure distribution in the structure of a propagating current sheet. *The Physics of Fluids*, 13(5):1303–1309, May 1970.

[52] T.E. Markusic and E.Y. Choueiri. Visualization of current sheet canting in a pulsed plasma accelerator. In 26^{th} *International Electric Propulsion Conference*, Kitakyushu, JAPAN, October 17-21 1999. IEPC 99-206.

[53] J.K. Ziemer, E.A. Cubbin, E.Y. Choueiri, and D. Birx. Performance characterization of a high efficiency gas-fed pulsed plasma thruster. In 33^{rd} *Joint Propulsion Conference*, Seattle, Washington, July 6-9 1997. AIAA 97-2925.

[54] W.J. Guman. Solid propellant pulsed plasma micro-thruster studies. In 6^{th} *Aerospace Sciences Meeting*, New York, New York, January 22-24 1968. AIAA 68-85.

[55] J.K. Ziemer and E.Y. Choueiri. Performance and erosion measurements of gas-fed pulsed plasma thrusters at NASA jet propulsion laboratory. Technical Report EPPDyL-JPL99a, Princeton University, March 1999.

[56] J. Blandino, D. Birx, J.K. Ziemer, and E.Y. Choueiri. Performance and erosion measurements of the pt8 gas-fed pulsed plasma thruster. Technical Report EPPDyL-JPL99b, NASA Jet Propulsion Laboratory, August 1999.

[57] J.K. Ziemer, E.Y. Choueiri, and D. Birx. Comparing the performance of co-axial and parallel-plate gas-fed PPTs. In 26^{th} *International Electric Propulsion Conference*, Kitakyushu, JAPAN, October 17-21 1999. IEPC 99-209.

[58] J.C. Keck. Current distribution in a magnetic annular shock tube. *The Physics of Fluids*, 5:630–632, 1962.

[59] F.J. Fishman and H. Petschek. Flow model for large radius-ratio magnetic annular shock-tube operation. *The Physics of Fluids*, 5:632–633, 1962.

[60] L. Liebing. Motion and structure of a plasma produced in a rail spark gap. *The Physics of Fluids*, 6:1035–1036, 1963.

[61] J.R. MacLelland, A.S.V. MacKenzie, and J. Irving. Schlieren photography of rail-tube plasmas. *The Physics of Fluids*, 9:1613–1615, 1966.

[62] W.H. Bostick. Hall currents and vortices in the coaxial plasma accelerator. *The Physics of Fluids*, 6(11):1598–1603, November 1963.

[63] R.B. Johansson. Current sheet tilt in a radial magnetic shock tube. *The Physics of Fluids*, 8(5):866–871, May 1965.

[64] M. Andrenucci, M. Caprili, and R. Lazzeretti. Theoretical performance of pulsed coaxial plasma guns. Technical report, Universita di Pisa, 1972.

[65] D. Keefer and R. Rhodes. Electromagnetic acceleration in pulsed plasma thrusters. In 25^{th} *International Electric Propulsion Conference*, Cleveland, Ohio, August 24-28 1997. IEPC 97-035.

[66] R.M. Patrick. High-speed shock waves in a magnetic annular shock tube. *The Physics of Fluids*, 2(6):589–598, November-December 1959.

[67] N.H. Kemp and H.E. Petschek. Theory of the flow in the magnetic annular shock tube. *The Physics of Fluids*, 2(6):599–608, November-December 1959.